CHEMISTRY
A EUROPEAN JOURNAL

DOI: 10.1002/chem.200900838

VIP

Dihydroxyacetone Phosphate Aldolase Catalyzed Synthesis of Structurally Diverse Polyhydroxylated Pyrrolidine Derivatives and Evaluation of their Glycosidase Inhibitory Properties

Jordi Calveras,[a] Meritxell Egido-Gabás,[b] Livia Gómez,[a] Josefina Casas,[b] Teodor Parella,[c] Jesús Joglar,[a] Jordi Bujons,*[a] and Pere Clapés*[a]

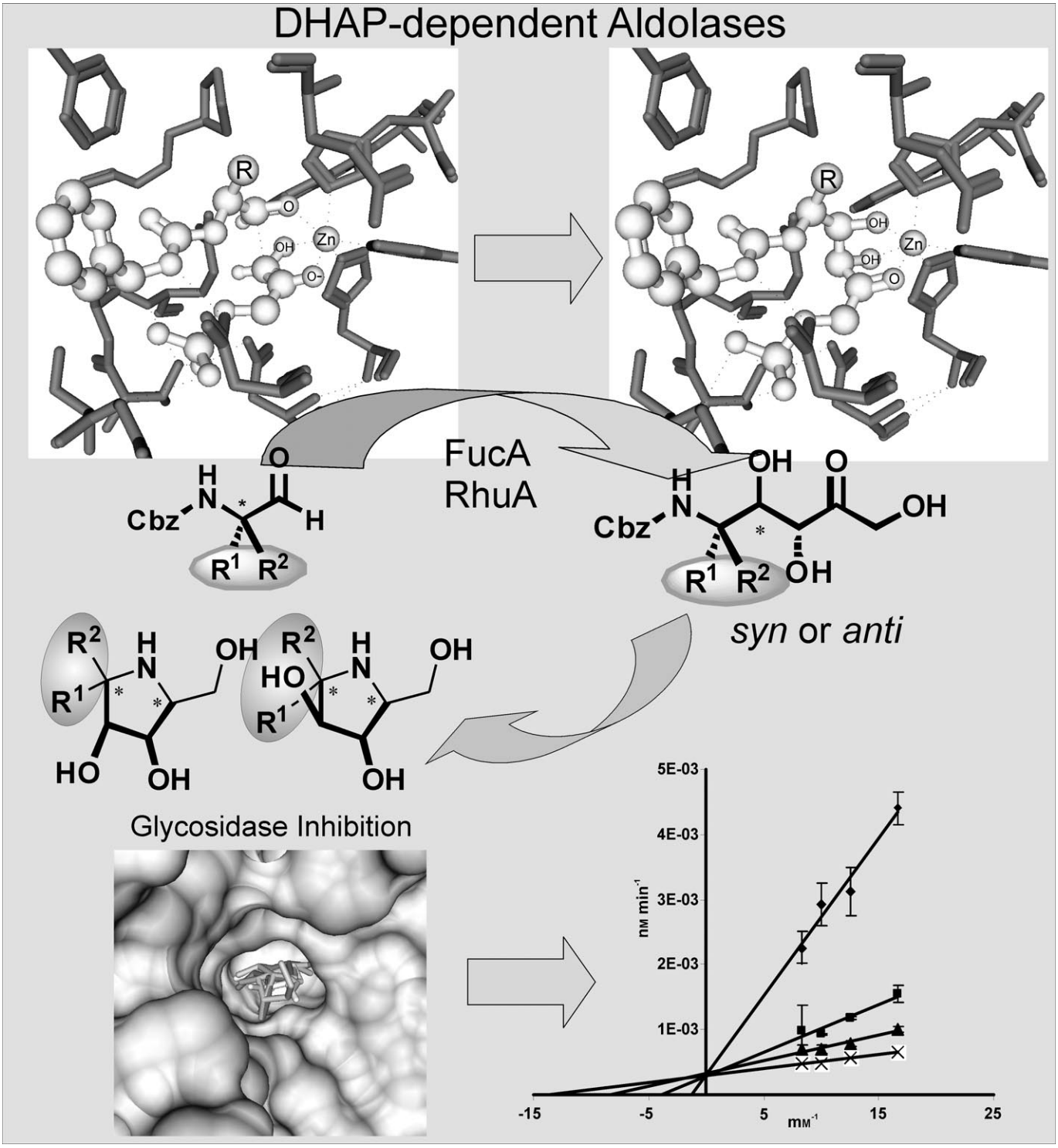

Abstract: The chemoenzymatic synthesis of a collection of pyrrolidine-type iminosugars generated by the aldol addition of dihydroxyacetone phosphate (DHAP) to C-α-substituted *N*-Cbz-2-aminoaldehydes derivatives, catalyzed by DHAP aldolases is reported. L-Fuculose-1-phosphate aldolase (FucA) and L-rhamnulose-1-phosphate aldolase (RhuA) from *E. coli* were used as biocatalysts to generate configurational diversity on the iminosugars. Alkyl linear substitutions at C-α were well tolerated by FucA catalyst (i.e., 40–70% conversions to aldol adduct), whereas no product was observed with C-α-alkyl branched substitutions, except for dimethyl and benzyl substitutions (20%). RhuA was the most versatile biocatalyst: C-α-alkyl linear groups gave the highest conversions to aldol adducts (60–99%), while the C-α-alkyl branched ones gave moderate to good conversions (50–80%), with the exception of dimethyl and benzyl substituents (20%). FucA was the most stereoselective biocatalyst (90–100% *anti* (3*R*,4*R*) adduct). RhuA was highly stereoselective with (*S*)-*N*-Cbz-2-aminoaldehydes (90–100% *syn* (i.e., 3*R*,4*S*) adduct), whereas those with *R* configuration gave mixtures of *anti*/*syn* adducts. For *i*Pr and *i*Bu substituents, RhuA furnished the *anti* adduct (i.e., FucA stereochemistry) with high stereoselectivity. Molecular models of aldol products with *i*Pr and *i*Bu substituents and as complexes with the RhuA active site suggest that the *anti* adducts could be kinetically preferred, while the *syn* adducts would be the equilibrium products. The polyhydroxylated pyrrolidines generated were tested as inhibitors against seven glycosidases. Among them, good inhibitors of α-L-fucosidase (IC_{50} = 1–20 μM), moderate of α-L-rhamnosidase (IC_{50} = 7–150 μM), and weak of α-D-mannosidase (IC_{50} = 80–400 μM) were identified. The apparent inhibition constant values (K_i) were calculated for the most relevant inhibitors and computational docking studies were performed to understand both their binding capacity and the mode of interaction with the glycosidases.

Keywords: aldol reaction · amino aldehydes · cyclitols · enzyme catalysis · glycosidase inhibitors

Introduction

Iminocyclitols are naturally occurring polyhydroxylated alkaloid mimics of glycosides.[1] Many of them are potent inhibitors of glycosidases and glycosyltransferases.[2] Glycoprocessing enzymes are interesting therapeutic targets as they are responsible for the metabolism of complex carbohydrate structures involved in many biochemical recognition processes. Glycosilation disorders affect to cell–cell communication, cell–matrix interaction, and immunological response; hence, they are related to diseases such as cancer, viral infections including HIV and hepatitis B and C, Gaucher and Fabry diseases, cystic fibrosis, carbohydrate deficiency syndrome (CDS), rheumatoid arthritis (chronic polyarthrithis), and IgA nephropathy (IgAN) among others.[3–6] Because of this, iminocyclitols have attracted much interest due to their potential therapeutic applications.[7–11] Furthermore, as transition-state mimics they constitute valuable probes in fundamental biochemical studies of glycosidase mechanism.[12,13]

Many efforts have been devoted to the synthesis of both natural and analogues of iminocyclitols with a wide variety of structures and substituents.[11,14–19] Importantly, generation of configurational diversity on the stereogenic centers appears to be of paramount importance to optimize their activity and selectivity.[20–23] Consequently, novel methodologies for the preparation of these compounds with a broad structural and configurational diversity are of increasing interest.

We have recently described a novel chemoenzymatic strategy to synthesize iminocyclitols of the piperidine and pyrrolidine type.[24,25] The key step of the strategy devised was the aldol addition of dihydroxyacetone phosphate (DHAP) to *N*-benzyloxycarbonylaminoaldehydes catalyzed by DHAP aldolases, such as D-fructose-1,6-diphosphate aldolase from rabbit muscle (RAMA), and L-rhamnulose-1-phosphate aldolase (RhuA) and L-fuculose-1-phosphate aldolase (FucA), both from *E. coli*. This methodology allowed us to prepare a number of iminocyclitols from *N*-Cbz-3-aminopropanal, *N*-Cbz-glycinal, and both enantiomers of *N*-Cbz-alaninal.

Therefore, it was regarded as both promising and significant to investigate the synthetic possibilities of the aforementioned strategy (Scheme 1) towards the preparation of novel pyrrolidine derivatives with potential new inhibitory properties against different glycosidases. Hence, in this work we endeavored first to gain insight into both tolerance and stereoselectivity of DHAP-dependent aldolases towards a structural variety of *N*-Cbz-aminoaldehydes, for a better understanding of their substrate specificity, and second to per-

[a] Dr. J. Calveras, L. Gómez, Dr. J. Joglar, Dr. J. Bujons, Dr. P. Clapés
Biotransformation and Bioactive Molecules group
Catalonia Institute for Advanced Chemistry-CSIC
Jordi Girona 18-26, 08034 Barcelona (Spain)
Fax: (+34) 932-045-904
E-mail: pere.clapes@iqac.csic.es

[b] Dr. M. Egido-Gabás, Dr. J. Casas
Research Unit for Bioactive Molecules (RUBAM)
Catalonia Institute for Advanced Chemistry-CSIC
Jordi Girona 18-26, 08034 Barcelona (Spain)

[c] Dr. T. Parella
Servei de Ressonància Magnètica Nuclear
Universitat Autònoma de Barcelona, Bellaterra (Spain)

Supporting information for this article is available on the WWW under http://dx.doi.org/10.1002/chem.200900838.

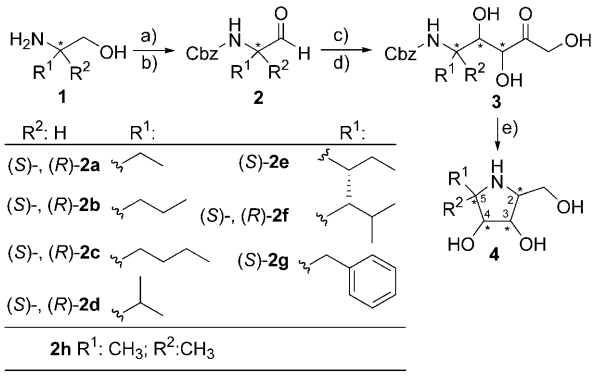

Scheme 1. Chemoenzymatic synthesis of structural diverse polyhydroxylated pyrrolidines: a) benzyloxycarbonylsuccinimide (Cbz-OSu) in dioxane, b) 2-iodoxybenzoic acid (IBX), AcOEt, reflux, c) DHAP, DHAP-dependent aldolase, d) acid phosphatase, e) Pd/C, H_2 (50 psi).

form a preliminary evaluation of the inhibitory properties of the products synthesized against seven glycosidases of different types and sources.

Results and Discussion

The iminocyclitols designed consist of polyhydroxylated pyrrolidine derivatives with different stereochemical configurations and different substituents at position C5 (Scheme 1) to explore their influence on their glycosidase inhibitory activity. Based on bibliographic data,[26–34] improvement of potency and selectivity against glycosidases and glycosyltransferases was observed when substituents close to the nitrogen atom were preferentially hydrophobic, aliphatic, or aromatic. The configuration of the stereogenic centers is of utmost importance for iminocyclitol inhibitors of glycoprocessing enzymes. Hence, stereocomplementary DHAP aldolases and the availability of pure *N*-Cbz-aminoaldehydes enantiomers may formally ensure a good configurational diversity. Thus, the selected aminoaldehydes (**2**) and the chemoenzymatic strategy are depicted in Scheme 1. D-Fructose-1,6-bisphosphate aldolase from rabbit muscle (RAMA) and L-rhamnulose-1-phosphate aldolase (RhuA) and L-fuculose-1-phosphate aldolase (FucA) from *E. coli* were the catalysts selected for the aldol addition of dihydroxyacetone phosphate (DHAP) to the *N*-Cbz-aminoaldehydes **2**. Treatment of aldol adducts **3** with acid phosphatase, followed by the removal of the Cbz and the intramolecular reductive amination with H_2 in the presence of Pd/C in a one-pot reaction furnished the pyrrolidine type iminocyclitols **4**. The configuration at positions C-3 and C-4 was controlled by the DHAP aldolase. The stereogenic center at C-2 was generated during the reductive amination and depends, in most cases, on the stereochemistry at C-4,[24,25] whereas the stereochemistry at C-5 is fixed by the starting aldehyde.

Enzymatic aldol additions of DHAP to *N*-Cbz-aminoaldehydes: The tolerance of the selected DHAP aldolases towards the *N*-Cbz-aminoaldehydes was investigated as a function of the reaction media, that is, high water content emulsions or 1:4 dimethylformamide/water mixtures.[25] Enzymatic aldol additions were running up to an apparent constant product concentration. When using RAMA as catalyst, no aldol adduct was detected with any of the selected *N*-Cbz-aminoaldehydes in any of the reaction systems assayed. This behavior was somehow predictable, considering the low conversion observed in a previous work during RAMA catalyzed aldolization of (*S*)- and (*R*)-*N*-Cbz-alaninal[25] and the fact that Lys107 and Arg109, located at the RAMA active site to fix its natural aldehyde acceptor, glyceraldehyde-3-phosphate, may hamper an effective interaction with hydrophobic C-α substituted aldehydes.

N-Cbz-Aminoaldehydes with linear alkyl C-α substituents (**2a–c**) were substrates for the FucA catalyst as well as those with C-α benzyl (**2g**) and dimethyl (**2h**) substituents (Figure 1). No product was detected in aldol additions with

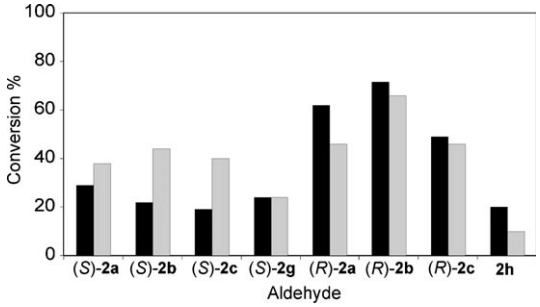

Figure 1. Molar percent conversions to products **3** from the aldol additions of DHAP to *N*-Cbz-aminoaldehydes ([DHAP] = 50 mM; [*N*-Cbz-aminoaldehydes] = 85 mM, the results at higher concentrations are summarized in Supporting Information) catalyzed by FucA in high water content emulsions (black bars) and in 1:4 DMF/water (grey bars). Conversions with respect to the starting DHAP concentration determined by HPLC of the crude reaction mixture using purified standards. Results in emulsions are the mean values (max. standard deviation < 5%) obtained in the three systems, $H_2O/C_{14}E_4$/tetradecane, $H_2O/C_{14}E_4$/hexadecane and $H_2O/C_{14}E_4$/squalane 90/4/6 wt% ($C_{14}E_4$: non-ionic polyoxyethylene ether surfactant, tetra(ethylene glycol)tetradecyl ether, $C_{14}H_{29}(OCH_2CH_2)_4OH$, with an average of 4 mol of ethylene oxide per surfactant molecule).

the *N*-Cbz-aminoaldehydes with branched alkyl C-α substituents, which appeared not to be tolerated by the FucA catalyst. In some instances, very small peaks appeared in the HPLC analysis (< 2% conversion) after long incubation times that were not identified, but might correspond to some aldol adduct formation.

Investigations of the reaction media: There is a remarkable effect of both the reaction media and aldehyde stereochemistry on the reaction conversion. Overall, (*R*)-*N*-Cbz-aminoaldehydes gave higher conversions than those with *S* configuration. Moreover, the best conversions with (*S*)- and (*R*)-*N*-Cbz-aminoaldehydes were achieved in 1:4 DMF/water and emulsions, respectively. It has been observed that organic solvent molecules, for example, DMF, cluster in the active

site of enzymes like elastase modifying the substrate–enzyme interactions in different ways.[35,36] If this may be extended to aldolases as well, DMF molecules at the FucA active site may facilitate the interaction of sterically unfavorable (*S*)-aldehydes.

RhuA was the most versatile aldolase accepting both linear and branched C-α substituted *N*-Cbz-aminoaldehydes (Figure 2).

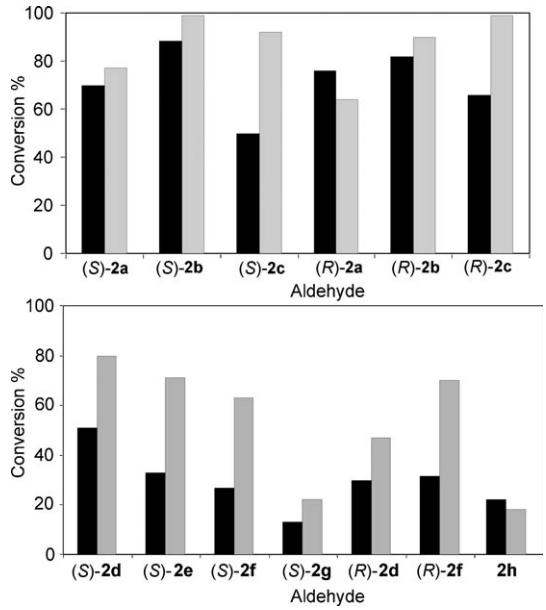

Figure 2. Molar percent conversions to products **3** in the aldol additions of DHAP to *N*-Cbz-aminoaldehydes ([DHAP] = 50 mM; [*N*-Cbz-aminoaldehydes] = 85 mM, the results at higher concentrations are summarized in Supporting Information) with linear (top) and branched (bottom) C-α substituents, catalyzed by RhuA in high water content emulsions (black bars) and in 1:4 DMF/water solution (grey bars). Conditions as explained in caption of Figure 1.

With the exception of the most hydrophobic butyl substituent, linear alkyl groups gave similar reaction conversions regardless of stereochemistry of aldehyde and reaction system used, while 1:4 DMF/water was the medium of choice for the sterically more demanding branched alkyl substituents. Furthermore, on increasing the reactant concentration up to [DHAP] = 100 mM and [*N*-Cbz-aminoaldehyde] = 170 mM (see Supporting Information) conversions for RhuA- and FucA-catalyzed reactions were generally higher in emulsion than those in 1:4 DMF/H_2O, probably because of the better solubilization properties of the former reaction medium.[37]

Investigations of temperature effects: Temperature effects were also investigated for RhuA aldolization of aldehydes (*R*)-**2a**, (*R*)-**2b** (vide infra), (*R*)-**2c**, (*R*)-**2f**, and (*S*)-**2f**. To this end, the selected reactions were conducted at 4 °C, because it has been reported that at this temperature the conversion achieved on FucA-catalyzed aldol addition of DHAP to (*R*)-*N*-Cbz-alaninal was significantly improved.[38] Interestingly, there were temperature effects on the stereoselectivity of the enzymatic reactions (vide infra), but no improvement on aldol conversions was observed for any of the selected examples, indicating that this phenomenon is not of general applicability.

Iminocyclitol synthesis: Aldol additions with selected aminoaldehydes catalyzed by RhuA and FucA were scaled up under the reactions conditions that provided the best conversions to *N*-Cbz-aminoketotriols **3**. The corresponding aldol adducts were purified from the excess of aldehyde and other byproducts. Special attention was paid to avoid the elimination of possible diastereoisomers formed during the enzymatic catalysis. Then, the isolated adducts were submitted to reductive amination following the methodology described by us.[24,25] The resulting iminocyclitols were fully characterized by NMR spectroscopy. The results, depicted in Table 1, show that epimeric mixtures at C-2 and C-4 were formed in some cases, indicating partial stereoselectivity in either the reductive amination or in the enzymatic aldol addition, respectively. Minor *N*-ethyliminosugars were also detected that were formed during the treatment with Pd/C as will be discussed below. Separation and purification of several of these mixtures was accomplished successfully by weak cation exchange chromatography on a CM-sepharose column in ammonium form. This allowed to set up an efficient purification procedure and to characterize the structure of the compounds in the mixtures unequivocally.

Stereochemistry of RhuA and FucA aldolases towards the *N*-Cbz-aminoaldehydes: The stereochemistry at C-4 of the iminocyclitols prepared accounted for the stereoselectivity of the aldolase–DHAP complex attack (i.e., nucleophile) on the carbonyl of the *N*-Cbz-aminoaldehydes.[24,25] This also may be an indication of the ability of the aldolase to fix the aldehyde in the right position during the donor attack in the active site. Remarkably, FucA catalyst gave excellent stereoselectivities, particularly towards the (*R*)-aldehydes (Figure 3), in good agreement with the previously reported FucA reactions with (*S*)- and (*R*)-*N*-Cbz-alaninal.[24] The pertinent conclusion was that the stereochemical outcome of FucA-catalyzed aldol additions of DHAP to C-α-substituted *N*-Cbz-aminoaldehydes is always *anti* (3*R*,4*R*), regardless of the structure and stereochemistry of the aldehyde.

RhuA displayed excellent stereoselectivity towards the *S* linear alkyl-substituted aldehydes, while significantly low for those with *R* configuration (Figure 4). In this respect, the amount of *anti* (3*R*,4*R*) configuration increased with the length of the alkyl chain, the (*R*)-butyl giving the inverted C-4 adduct (i.e., FucA stereochemistry) as major product (Figure 4A).

The same trend was observed with C-α-branched alkyl substituents (Figure 4B). Interestingly, (*S*)-**2d** gave the expected aldol adduct with 4*S* stereochemistry, whereas its enantiomer (*R*)-**2d** gave the opposite 4*R* adduct, both as single diasteromers. Therefore, RhuA displayed an excellent stereoselectivity for these reactions.

Table 1. Structures of iminosugars and stereoisomeric ratio ascertained by NMR spectroscopy from the strategy depicted in Scheme 1.

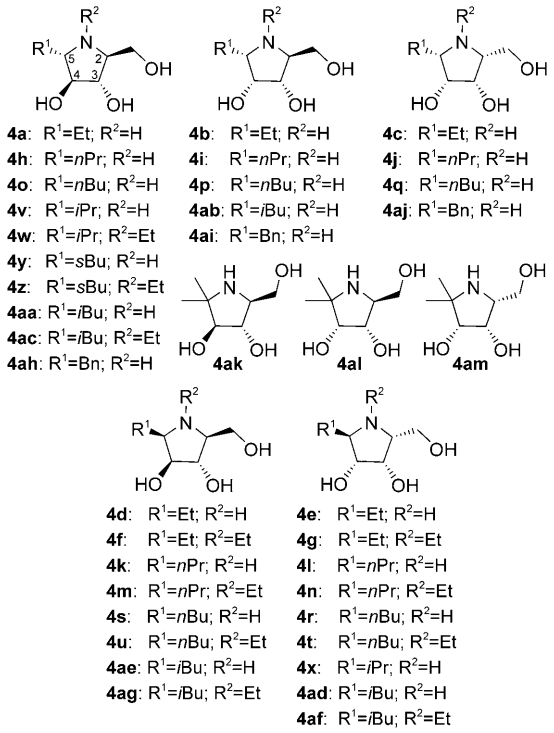

Entry	Aldehyde	Aldolase	Product (ratio)
1	(*S*)-**2a**	RhuA	**4a** (100)
2	(*S*)-**2a**	FucA	**4a/4b/4c** (10:86:4)
3	(*R*)-**2a**	RhuA	**4d/4e/4f/4g** (48:30:11:11)
4	(*R*)-**2a**	FucA	**4e** (100)
5	(*S*)-**2b**	RhuA	**4h** (100)
6	(*S*)-**2b**	FucA	**4h/4i/4j** (4:86:10)
7	(*R*)-**2b**	RhuA	**4k/4l/4m/4n** (44:34:11:10)
8	(*R*)-**2b**	FucA	**4l** (100)
9	(*S*)-**2c**	RhuA	**4o/4p** (93:7)
10	(*S*)-**2c**	FucA	**4o/4p/4q** (10:80:10)
11	(*R*)-**2c**	RhuA	**4s/4r/4t/4u** (28:63:5:5)
12	(*R*)-**2c**	FucA	**4r** (100)
13	(*S*)-**2d**	RhuA	**4v/4w** (84:16)
14	(*R*)-**2d**	RhuA	**4x** (100)
15	(*S*)-**2e**	RhuA	**4y/4z** (55:45)
16	(*S*)-**2f**	RhuA	**4aa/4ab/4ac** (71:6:23)
17	(*R*)-**2f**	RhuA	**4ae/4ad/4af/4ag** (32:43:16:9)
18	(*R*)-**2f**	RhuA	**4ad**[a] (100)
19	(*S*)-**2g**	RhuA	**4ah** (100)
20	(*S*)-**2g**	FucA	**4ai/4aj** (62:38)
21	**2h**	RhuA	**4ak/4al** (83:17)
22	**2h**	FucA	**4al/4am** (44:56)

[a] Synthesis conducted at 4 °C.

Investigations of temperature effects: The effect of temperature on this stereoselectivity was also investigated as a function of the *N*-Cbz-aminoaldehyde. For instance, no changes were observed with (*R*)-**2c**, whereas an increase of the *anti* (3*R*,4*R*) configuration from 44 to 61 % was found for (*R*)-**2b** when cooling down from 25 to 4 °C, respectively. The most significant result was obtained with (*R*)-**2f**: at 25 °C it gave a 55:45 *anti*:*syn* ratio, whereas at 4 °C only the *anti* product

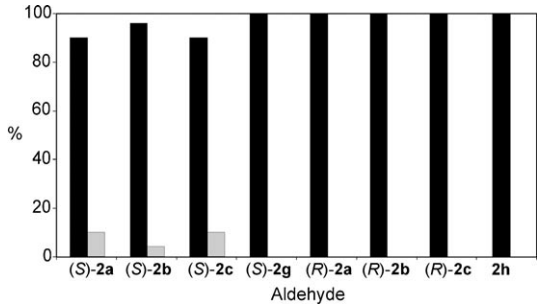

Figure 3. Stereoselectivity of FucA catalysis in the aldol additions of DHAP to *N*-Cbz-aminoaldehydes. Percentage of adducts *anti*, that is, (3*R*,4*R*)-**3** (or (3*S*,4*R*) in the iminosugar, black bars), and *syn*, that is, (3*R*,4*S*)-**3** (or (3*S*,4*S*) in the iminosugar, grey bars), for each aldehyde acceptor.

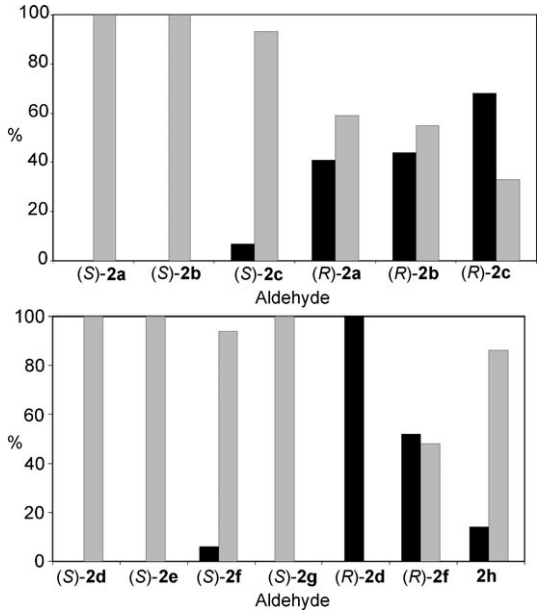

Figure 4. Stereoselectivity of RhuA catalysis towards the *N*-Cbz-aminoaldehydes with linear (top) and branched (bottom) C-α substituents. Percentage of adducts *anti*, that is, (3*R*,4*R*)-**3** (or (3*S*,4*R*) in the iminosugar, black bars), and *syn*, that is, (3*R*,4*S*)-**3** (or (3*S*,4*S*) in the iminosugar, grey bars), for each aldehyde acceptor.

was detected. This result indicates that the *anti* aldol adduct was kinetically preferred and that a reduction of the temperature increased the stereoselectivity, as was also observed in other aldolases.[39]

Molecular modeling: Molecular modeling studies were carried out to substantiate this hypothesis. Thus, an exhaustive conformational analysis was carried out for the *syn* and *anti* adducts derived from the (*S*)-**2c**, (*R*)-**2c**, (*S*)-**2d**, and (*R*)-**2d** aldehydes, as representative examples, using a combination of the systematic and stochastic conformational search algorithms implemented in the program MOE (Chemical Computing Group, Montreal), as previously described.[24,40] Table 2 summarizes the difference in calculated energies for

Table 2. Energy difference [kcal mol^{-1}] of the global minima determined for the *syn* and *anti* adducts derived from aldehydes **2c** and **2d**, in the free state and bound in the RhuA active site. Energies determined with the MMFF94x forcefield under continuum water solvation conditions, as detailed in Experimental Section.

Aldehyde	Free adduct $\Delta E^{syn-anti}$	RhuA-adduct complex $\Delta E^{syn-anti}$
(*R*)-**2c**	−4.3	18.2
(*S*)-**2c**	−3.1	12.9
(*R*)-**2d**	−5.1	23.6
(*S*)-**2d**	−0.7	34.1

the global minima determined for each pair of *syn–anti* adducts ($\Delta E^{syn-anti}$) and the corresponding geometries are reported in the Supporting Information. From these values it is clear that the *syn* adducts are thermodynamically favored, assuming similar entropic contributions to ΔG, by −3.3 kcal mol^{-1} on average for the compounds considered. This value correlates well with the stereochemistries observed for the aldol adducts obtained from (*S*)-aldehydes with RhuA catalysis. Similar results were already reported by us for a small set of aldol adducts derived from *N*-protected 3-aminopropanal.[40]

We also looked at the complexes of the above adducts in the active center of RhuA. Figure 5 shows the lowest energy conformers obtained for the *syn* and *anti* adducts from aldehydes (*S*)-**2c** and (*S*)-**2d** bound in the active center of RhuA. The modeled structures show that the aldol reaction products coordinate to the active site metal simultaneously with the oxygen atoms of the C-2 carbonyl and the C-3 and C-4 hydroxyl groups, thus providing a hexacoordinate environment to the essential Zn^{2+}, with the participation of the histidines at positions 141, 143, and 212 of the protein. Similar geometries were obtained for the adducts derived from (*R*)-**2c** and (*R*)-**2d**. This arrangement resembles that found in the crystal structure of RhuA-phosphoglycolohydroxamate complex (PDB 1GT7), in which a water molecule coordinates the cation in addition to the two oxygen atoms from the ligand. In a very recent paper in which high-level computations have been used to study the enzymatic mechanisms of RhuA and FucA, Jiménez et al.[41] have shown that in the transition state for the C–C formation step, a negative charge builds up on the aldehyde oxygen atom, which is stabilized by interaction with the positive charge of the Zn^{2+}, and that this interaction is maintained by the aldol product.

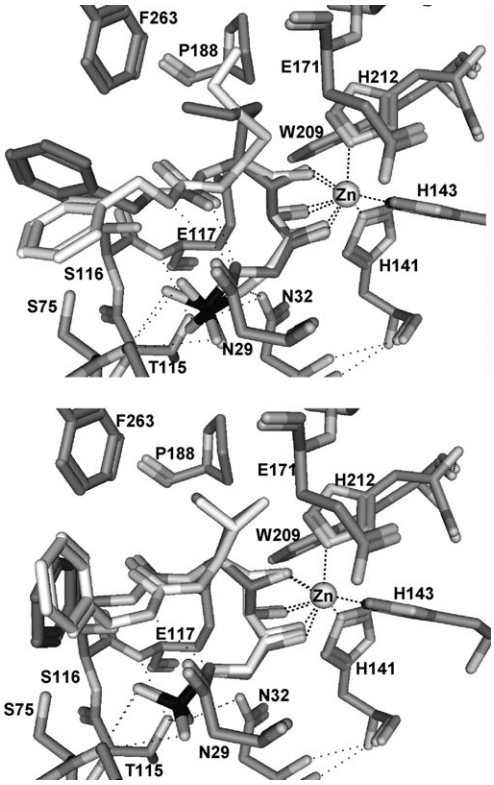

Figure 5. Structural models of the *syn* (dark grey) and *anti* (light grey) adducts derived from aldehyde (*S*)-**2c** in the active center of RhuA (top), and the *syn* (dark grey) and *anti* (light grey) adducts derived from aldehyde (*S*)-**2d** in the active center of the same enzyme (bottom). The corresponding color figure is available in the Supporting Information.

Our models for the RhuA-adduct complexes gave the energy differences between the *syn* and *anti* products, which are summarized in Table 2. The *anti* adduct complexes were always lower in energy than the corresponding *syn* ones, apparently due to more strained geometries for the later. Determination of the actual energy differences between transition states would require of accurate quantum mechanics calculations. However, it seems plausible that since the geometries of the transition states for the C–C bond formation reactions are similar to those of the aldolase adduct complexes,[41] the $\Delta E^{syn-anti}$ values of Table 2 could correlate with the energy differences for the corresponding transition states. Therefore, these results would suggest lower activation barriers for the *anti* adducts and, consequently, a kinetic preference for these, which could explain the formation of larger proportions of *anti* products from aldehydes (*R*)-**2c** or (*R*)-**2d**. If this can be extended to the other aldehydes, it would provide an explanation to the experiments carried out at low temperature.

Reductive amination: Conversion of the corresponding adducts to polyhydroxylated pyrrolidine derivatives **4** by Pd/C catalyst in the presence of H_2 (50 psi) gave in most cases the expected 2-OH/4-OH *syn* configuration. On the other hand, aldol adducts with 3*R*,4*R*,5*S* configuration gave five-membered ring iminosugars with 2-OH/4-OH *anti* configuration as major product (Table 1, entries 2, 6, and 10). Exceptions to this were the aldol adducts from the aldehydes (***S***)-**2g** and **2h**, for which limited or no stereoselectivity was observed (Table 1, entries 20 and 22).

Minor amounts of *N*-ethylated byproducts may account for a reductive amination of ethanal and the iminosugar. The ethanal was formed in situ by Pd-catalyzed oxidation of ethanol from the solvent mixture in presence of dissolved oxygen[42] and before H_2 addition. This side reaction was avoided if the oxygen dissolved of the reactants solution was displaced by bubbling with N_2 gas prior to the addition of Pd/C catalyst.

NMR studies: Similar to the NMR study on the iminocyclitols obtained in previous papers,[24,25] and as a complement to NOE data, the shielding effects were also used as a probe to assign the relative stereochemistry (Table 3 in the Supporting Information). Differences on the ^{1}H chemical shift were observed depending on the protonation state of the imino group. The protonated imino group induced 0.1–0.5 ppm upfield shift on protons of the molecule (see Supporting Information). This was useful in some cases to separate unresolved signals. Remarkably, the NMR analysis of **4z** and **4ac** revealed the presence of two conformers depending on the protonation of the imino group. When the imino group existed as free base the spectra showed signals assigned unequivocally to the product, while when the imino group was protonated, the spectrum showed the presence of two groups of signals corresponding to the two conformers of the product (see Supporting Information).

Preliminary inhibitory properties against glycosidases: The compounds, synthesized both in pure form and as mixtures, were assayed as inhibitors of commercial glycosidases: α-D-glucosidase from baker's yeast, β-D-glucosidase from sweet almonds, β-D-galactosidases from bovine liver and *Aspergillus oryzae*, α-L-fucosidase from bovine kidney, α-L-rhamnosidase from *Penicillium decumbens*, and α-D-mannosidase from jack bean. A cursory inspection of IC_{50} values (Figure 6) indicated that among the iminocyclytols synthesized, there are good inhibitors of α-L-fucosidase (IC_{50} = 1–20 μM), moderate inhibitors of α-L-rhamnosidase (IC_{50} = 7–150 μM) and poor inhibitors of α-D-mannosidase (IC_{50} = 80–400 μM). Furthermore, none of them had inhibitory properties against α-D-glucosidase from baker's yeast, β-D-glucosidase from sweet almonds, and β-D-galactosidases from bovine liver and *A. oryzae*. Next, K_i and type of inhibition were determined for the most active compounds or mixtures (Table 3). Mixtures showing a poor or null inhibitory activity were not further processed.

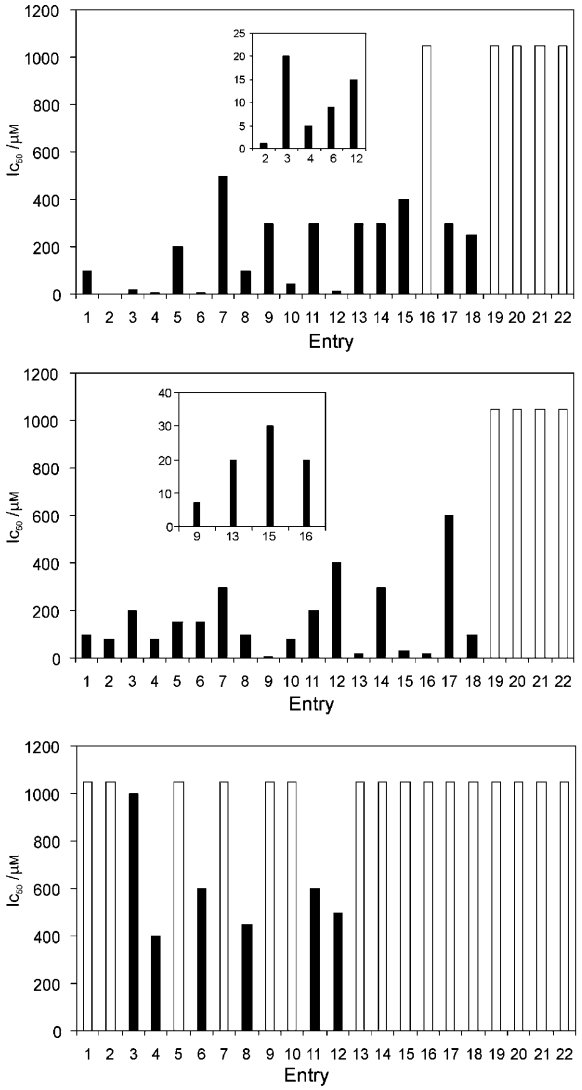

Figure 6. IC_{50} values of the compounds synthesized for the inhibition of α-L-fucosidase from bovine kidney (top), α-L-rhamnosidase from *P. decumbens* (middle), and α-D-mannosidase from jack bean (bottom). Empty bars: no inhibition.

Table 3. Activities of the compounds synthesized. IC_{50} and K_i values of the most active compounds against: α-L-fucosidase from bovine kidney, α-L-rhamnosidase from *P. decumbens*, and α-D-mannosidase from jack bean.

	IC_{50} [μM]			K_i [μM]		
	α-L-fucosidase	α-L-rhamnosidase	α-D-mannosidase	α-L-fucosidase	α-L-rhamnosidase	α-D-mannosidase
4a	100	100	ni[f]	nd[g]	nd	–
4b[a]	0.6	80	ni	0.30 ± 0.10	109 ± 6	–
4c[a]	1	ni	ni	0.35 ± 0.15	–	–
4e[a]	5	80	400	7.6 ± 0.5	49 ± 4	137 ± 5
4h	200	150	ni	nd	62 ± 6	–
4i[a]	9	150	ni	7.0 ± 0.7	nd	–
4l	100	100	450	nd	nd	305 ± 10
4o[b]	300	7	ni	nd	4.8 ± 0.6	–
4p[c]	40	80	ni	8.5 ± 0.8	131 ± 8	–
4r	15	400	500	22 ± 4	nd	373 ± 15
4v[d]	300	20	ni	nd	26 ± 4	–
4y[a]	ni	30	ni	–	55 ± 5	–
4aa[e]	ni	20	ni	–	25 ± 4	–

[a] Purified as described in the Experimental Section. [b] Purity 93% (entry 9, Table 1). [c] Purity 80% (entry 10, Table 1). [d] Purity 84% (entry 13, Table 1). [e] Purity 71% (entry 16, Table 1). [f] ni = no inhibition. [g] nd = not determined.

Inhibitory properties of the compounds against α-L-*fucosidase from bovine kidney*: The compounds given in entries 2, 3, 4, 6, 10, and 12 (Table 1) inhibited α-L-fucosidase in a competitive manner. The iminosugars from entry 2, the mixture with the highest activity, were isolated and purified, and their inhibitory properties against α-L-fucosidase evaluated. Compounds **4b** and **4c**, were the most potent among those obtained in this work (Table 3), whereas **4a**, which was also obtained in entry 1, was much less active. The related compounds 2,5-imino-1,2,5-trideoxy-L-altritol (**5**) and 2,5-dideoxy-2,5-imino-L-fucitol (**6**), analogues of **4b** and **4c**, respectively by which carry a 5-methyl substituent instead of the ethyl group, were found to be more potent α-L-fucosidase inhibitors with, $K_i = 80$ and 4.9 nM, respectively.[43,44]

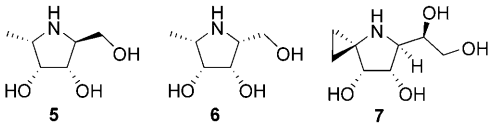

The activity of compound **6**, not previously reported to the best of our knowledge, is amongst the highest reported for pyrrolidine and piperidine type iminosugars.[45–49] Other pyrrolidine derivatives with similar stereochemistry (i.e., 3*S*,4*R*,5*S*) have also been reported as strong inhibitors of α-L-fucosidase,[50–52] while some diastereomerically related isomers of **5** and **6** have shown much lower activities (e.g. $K_i =$ 165 μM for the 2*R*,3*R*,4*R*,5*R* isomer[46]), suggesting a strong stereochemical demand of the α-L-fucosidase active site. In this sense, looking at the compounds synthesized in this work, modification of the stereochemistry at C-5 from *S* to *R*, for example, compare **4c** versus **4e**, or at C-4 from *R* to *S*, for example, compare **4b** versus **4a**, **4i** versus **4h**, or **4p** versus **4o**, result in moderate to large decreases of the inhibitory activity (Table 3).

On the other hand, increasing the length of the substituent at C-5 from methyl (e.g., **5** and **6**) to ethyl (e.g., **4b** and **4c**), propyl (e.g., **4i**), or butyl (e.g., **4p**) implied a progressive loss of inhibitory activity. Furthermore, benzyl or dimethyl substituents at C-5, (e.g., entries 19–22) completely suppressed the activity of the corresponding pyrrolidine derivatives (Figure 5, top). Altogether, these results suggest a relatively small hydrophobic pocket in the active site of α-L-fucosidase, which could be occupied by small substituents on C-5 position, but not the larger ones. In this respect, Laroche et al.[53] described a spirocyclopropyl pyrrolidine (**7**) as a competitive inhibitor ($K_i = 1.6$ μM). The sterically more restricted cyclopropane group may be better accommodated in this hydrophobic core than the dimethyl group (entries 21 and 22) and effectively interact with the enzyme active site.

Although no fucosidase structure of mammalian origin is available up to date in the Protein Data Bank, the structure of α-L-fucosidase from *Thermotoga maritima* has recently been reported.[54] The sequence of this bacterial enzyme exhibits 34–38% identity to the sequences of α-L-fucosidases from animals, and of the 13 residues that constitute the active site cavity, 11 are conserved in the human protein. Furthermore, homology modeling suggested a high similarity between the shapes of the catalytic center of both the bacterial and human proteins, while larger differences were found in the aglycone binding site.[54] Consequently, the structure of α-L-fucosidase from *T. maritima* was used as a reasonable model to carry computational docking studies that help to understand the fucosidase binding capacity and the way of interaction of the pyrrolidine inhibitors identified.

Figure 7 shows the best docked poses obtained for the α-L-fucosidase active compounds **6** and **4b** and the less active **4r**, as well as the experimentally determined structure of L-fucose bound into the active center of α-L-fucosidase from *T. maritima*, for the sake of comparison. The pyrrolidine inhibitors occupy the catalytic site in a similar manner as the crystallized ligand and establish a strong interaction between their protonated imine group and the catalytic E266 residue.

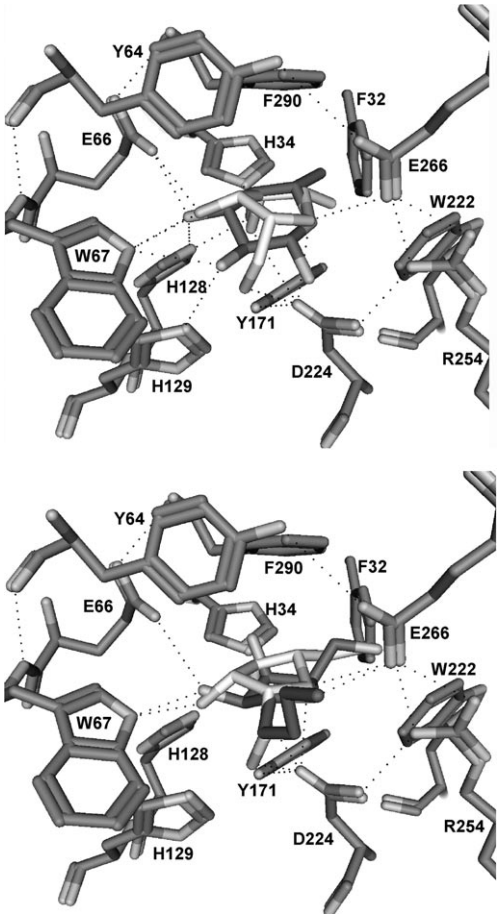

Figure 7. Top: Crystal structure of L-fucose (dark grey) bound in the active center of α-L-fucosidase from *T. maritima* (PDB 1ODU) and best docked pose obtained for **6** (light grey). Bottom: Best docked poses obtained for **4b** (light grey) and **4r** (dark grey) in the active center of the same enzyme. The corresponding color figure is available in the Supporting Information.

However, the methyl group of **6** and the ethyl group of **4b** are directed towards the inner part of the cavity, where there is a relatively small hydrophobic pocket constituted by residues F32, Y171, F290, and W222, while **4r** shows an inverted orientation, with its larger butyl substituent pointing towards the external opening of the binding pocket. The interaction diagram for **6** (see Supporting Information) shows extensive hydrogen-bonding interactions with residues H34, E66, W67, H128, H129, D224, and E266, while the slightly displaced conformation of **4b**, required to allocate the larger ethyl group in the hydrophobic cavity, shows hydrogen bonding with residues W67, H129, D224, and E266. The even larger size of the butyl group, which forces **4r** to adopt an inverted conformation, only allows for hydrogen bond interactions with residues W67 and E266. This trend, that is, smaller alkyl chains (methyl, ethyl, or propyl) located in the hydrophobic cavity and larger chains (butyl or benzyl) oriented towards the solvent exposed entry to the cavity, is observed for most of the compounds considered in our docking studies (see Supporting Information). Therefore, the determined binding modes for these compounds are in good agreement with the observations suggesting a steric impediment for bulky substituents at the pyrrolidine C-5 position and lower activities with increasing size of the substituents at that position. Indeed, the scores derived from the estimation of the interaction energies (MM/GBVI scores, see Experimental Section) between the inhibitors and the α-L-fucosidase correlate reasonably well with the free energies of binding calculated from the inhibition data (Table 4 and Figure 8). Although this correlation could be improved if the structural differences between the α-L-fucosidase from *T. maritima* and the bovine enzyme were considered, it does reflect a plausible binding mode for pyrrolidine type inhibitors that might probably be conserved for both α-L-fucosidases. Better accounting for other factors like the entropic contribution to binding or the differences in solvation–desolvation energies among the different compounds, recently shown as having an enormous contribution to ligand binding among glycosidase inhibitors,[55] would also have a large impact to improve such correlation. Work in this sense is actually being carried out by our group.

Table 4. Free energies of binding determined from the experimental K_i values and docking MM/GBVI scores.

	ΔG^{exptl} [K cal mol^{-1}]	MM/GBVI score		ΔG^{exptl} [K cal mol^{-1}]	MM/GBVI score
4a	−5.46[a]	−25.4	**4r**	−6.35	−20.7
4b	−8.90	−25.3	**4aj**	–	−24.5
4c	−8.81	−26.5	**4am**	–	−19.9
4e	−6.98	−25.3	**5**	−9.68	−29.2
4i	−7.03	−23.4	**6**	−11.34	−30.7
4p	−6.92	−25.1	**7**	−7.91	−25.8

[a] Calculated from the IC_{50} value.

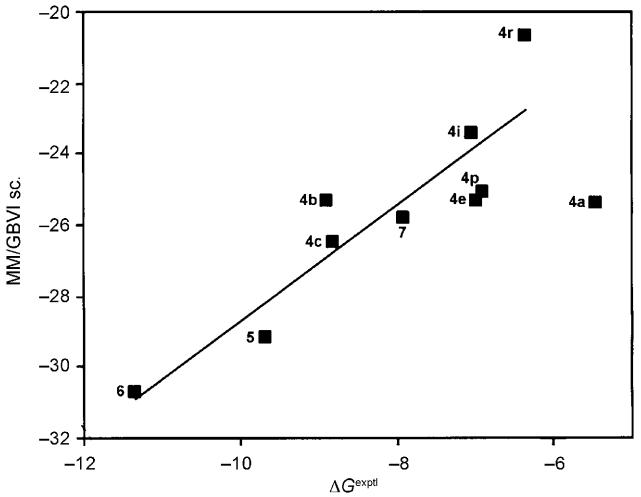

Figure 8. Correlation between Δ^{Gexptl} and MM/GBVI scores from Table 4.

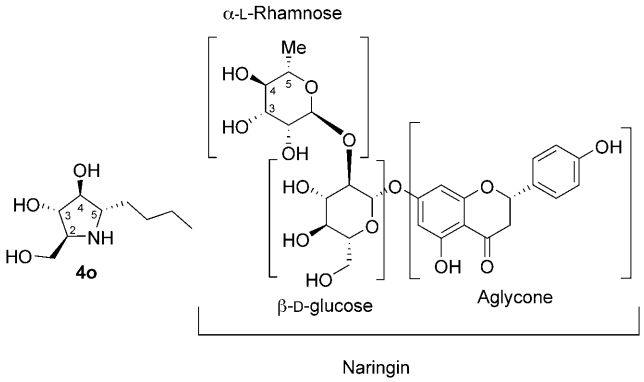

Inhibitory properties of the compounds against α-L-rhamnosidase from Penicillium decumbens: Compound **4o** was the most potent α-L-rhamnosidase inhibitor found among the iminosugars synthesized in this work ($K_i = 4.8$ μM). It has been suggested that the α-L-rhamnosidase inhibition shown by some pyrrolidines can be rationalized in terms of stereochemical similarities with α-L-rhamnose.[56,57] Considering the structure of naringin, a natural substrate of α-L-rhamnosidase, it is apparent that the stereochemistry of **4o** (i.e., 2*S*,3*S*,4*S*,5*S*) matches that of the rhamnose moiety at C-3, C-4, and C-5. This would place the 5-butyl group of **4o** on the same location as the 5-methyl group of rhamnose. A similar reasoning was argued by Chapman et al. to explain the α-L-rhamnosidase inhibitory activity of **8** ($K_i = 3.0$ μM).[56] However, Kim et al. proposed a role as aglycone for hydrophobic substituents at C-2 of pyrrolidines such as **9** ($K_i = 3.4$ μM).[57]

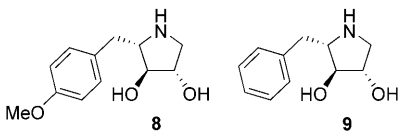

The lack of structural data for α-L-rhamnosidase from *P. decumbens* precludes a definitive answer about the binding mode of pyrrolidine inhibitors into the active center of the enzyme. In this sense, the crystal structure of an α-L-rhamnosidase from *Bacillus* sp. GL1 (RhaB) has recently been solved.[59] This enzyme exhibits a slight identity with the known sequences of α-L-rhamnosidases from fungi (i.e., 24% with RhaA and RhaB of *Aspergillus aculeatus*, or 20% with RamA of *Clostridium stercorarium*).[60] However, the fact that it shows activity against the common substrate naringin suggests that its catalytic site should share similar shape and structural features with other α-L-rhamnosidases like that of *P. decumbens*. Therefore, we carried out docking experiments with the structure of RhaB from *Bacillus* sp. GL1 to shed light about the binding mode of pyrrolidine **4o**. Figure 9 (top) shows the best three poses obtained for this compound, which differ slightly but establish essentially the same interactions with the enzyme. Unlike for the case of α-L-fucosidase, these docking results suggest that **4o** could bind into the α-L-rhamnosidase active site orienting the butyl substituent towards the inside of the enzyme cavity, in a hydrophobic subsite made up of W576, I626, W629, W679, and L681, which has been proposed as the recognition site for the methyl group of the rhamnosyl moiety.[59] The protonated imine group of the inhibitor establishes a strong interaction with the essential E572 residue, while the hydroxyl groups at C-1, C-3, and C-4 can establish diverse hydrogen-bond interactions with residues Q147, N849, and R858.

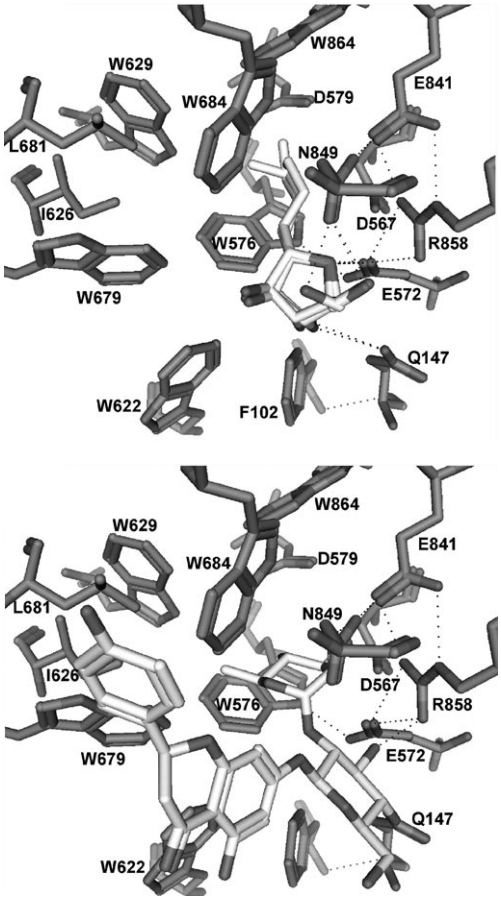

Figure 9. Representation of the active site of α-L-rhamnosidase from *Bacillus* sp. GL1 with the three best docked conformations obtained for pyrrolidine **4o** (light grey; top), and the best docked pose obtained for naringin (light grey; bottom). The corresponding color figures are available in the Supporting Information. It is apparent on both representations the presence, at the center-left side, of a number of residues (F102, W576, W622, I626, W629, W679, L681, W684 and W864) that constitute a relatively large hydrophobic subcavity, while the center-right side is essentially constituted by polar residues (Q147, D567, E572, D579, E841, N849 and R858) that can establish multiple hydrogen bonds with the substrates and the inhibitors.

Naringin was also docked in the active center of α-L-rhamnosidase (Figure 9, bottom) for comparison purposes, since there is no structure available in the PDB of the enzyme with a bound rhamnosyl derivative or inhibitor. The best docked pose obtained constitutes a plausible geometry for this substrate, with the reactive C-1 and 1,2-β-glycosidic oxygen atoms located close to the essential E572, the rhamnose moiety parallel to the ring of W576, fixed by hydrophobic stacking, and its methyl group oriented towards the hydrophobic residues I626, W679, and L681.[59] Comparing this docked naringin with the docked conformations obtained for **4o**, it becomes apparent that the size of the butyl chain forces some displacement of the pyrrolidine ring away from the rhamnose location and towards the entrance to the cavity. This causes a lack of coincidence of the hydroxyl groups at C-3 and C-4 of the inhibitor with those of the rhamnose moiety of naringin. However, it should be kept in mind that the pyrrolidine inhibitors, containing a protonated imino group, are thought to mimic the enzyme transition-state complex rather than enzyme–substrate complex. Nonetheless, the orientation of the alkyl chain towards the hydrophobic subcavity in the catalytic site, resulting in a more efficient binding for compounds with larger hydrophobic chains, correlates with the observation that decreasing the C-5 chain length from butyl to propyl (**4h**), ethyl (**4a**) or methyl (**10**; $K_i = 43$ μM)[25] led to a loss of inhibitory capacity. Branched alkyl chains on C-5, for example, compounds **4v**, **4y** and **4aa**, showed some inhibitory properties, but always lower than those of **4o**, likely reflecting additional steric requirements of the biding site. In this sense, the C-5 dimethyl substituted pyrrolidines, entries 19–22, were not inhibitors of α-L-rhamnosidase. This is in contrast with the activities observed for compounds such as **8** and **9**, which are analogues of **4ah**. The lack of activity of **4ah** suggests that the hydroxymethyl moiety present in this pyrrolidine might have a deleterious effect on the activity against the enzyme. This effect could also contribute to the lower activity observed for **4a** or **10** compared to their counterparts **11**[58] or **12**[56] ($K_i = 5.5$ and 5.9 μM, respectively).

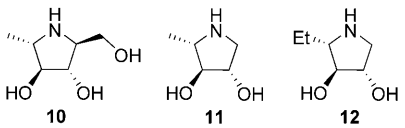

Inhibitory properties against α-D-mannosidase from jack bean: The compounds synthesized showed weak inhibitory properties against α-D-mannosidase. Pyrrolidine derivatives with 2*R*,3*S*,4*R*,5*R* configuration and linear alkyl substituents on C-5 (synthesized compounds with general structure **15**, e.g., **4e**, **4l**, and **4r**) were the best competitive inhibitors among the compounds synthesized. These compounds show a *cis* arrangement of their hydroxyl groups at C-3 and C-4, which parallels that of the hydroxyl groups at C-2 and C-3 of α-D-mannose (**13**) and other known pyrrolidine inhibitors of α-D-mannosidase like mannostatin A (**14**). These *cis*-arranged hydroxyl groups are known to coordinate the essential Zn^{2+} present in the active center of the related α-D-mannosidase from *D. melanogaster*,[61–64] which is a class II α-D-mannosidase belonging to glycosyl hydrolase family 38 (Carbohydrate Active Enzymes database, http://www.cazy.org)[65] as the α-D-mannosidase from jack bean. Both α-D-mannosidases show the characteristic IDPFGH sequence in their active site,[66] which is highly conserved among all class II α-D-mannosidases, and both are inhibited similarly by compounds like mannostatin and swainsonine. Therefore, the structure of the α-D-mannosidase from *D. melanogaster* was used to model the binding of the pyrrolidines synthesized in this work.

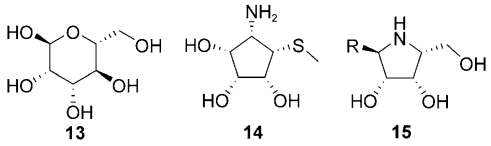

Figure 10 shows the docking results obtained for **4e** and **4r**, which were very similar to those found for **4l** (not shown), as well as the experimentally determined structures of mannose and mannostatin A bound in the active center of α-D-mannosidase from *D. melanogaster*, for comparison. The docking poses found for the pyrrolidines share a similar binding mode with mannose and mannostatin A, coordinating the Zn^{2+} with the hydroxyl groups at C-3 and C-4 and hydrogen bonding to residues D92, D204, D472, and Y727. They also establish a strong interaction between the protonated imine and the negatively charged D204, similar to those found between the charged amino group of mannostatin A and the catalytic acid residues D204, D341, and Y269.[62] However, the hydrophobic chains of **4e** and **4r** are oriented towards the water-accessible opening of the cavity and not towards the hydrophobic pocket constituted by residues F206, W415, and Y727, in which the thiomethyl group of mannostatin A is located.[62, 67] The interaction of this methyl group with the hydrophobic residues seems to contribute importantly to the high potency of mannostatin A. Furthermore, it allows the right orientation of the unpaired electrons of the sulfur atom, such that they can interact with the backbone of residue R876, which seems to be a critical determinant of potency.[62] Therefore, the lack of these important interactions together with the unfavorable exposure

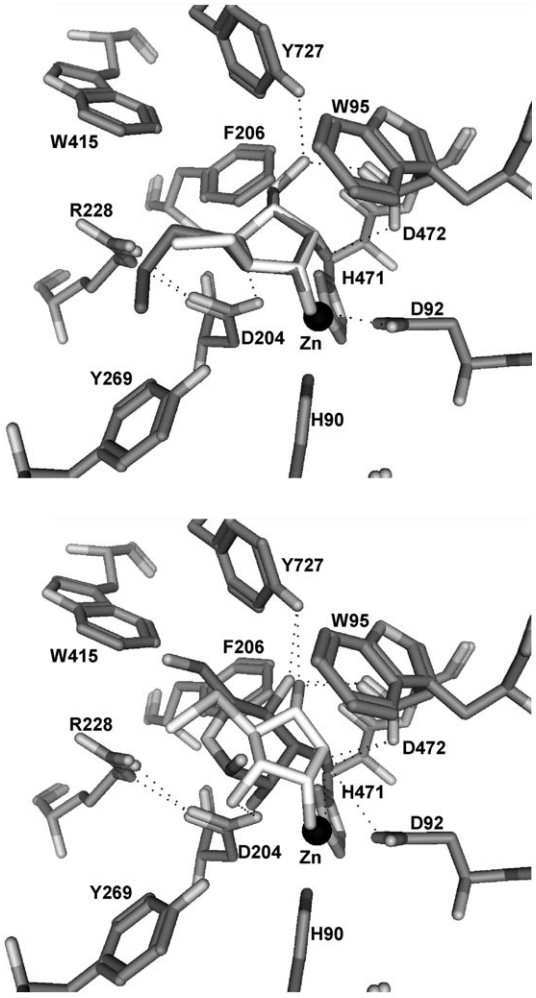

Figure 10. Top: Best docked poses obtained for compounds **4e** (light grey) and **4r** (dark grey) in the active site of α-D-mannosidase from *D. melanogaster*. Bottom: Bound conformations of mannostatin A (light grey) and mannose (dark grey) in the active center of the same enzyme (PDB 2F7O and 3BUQ, respectively).[67] The corresponding color figures are available in the Supporting Information.

of their hydrophobic chain to the solvent could explain the low activity observed for pyrrolidines **4e**, **4l**, and **4r**. Substituting the linear by branched alkyl chains, for example, **4x** and **4ad**, abolish completely the inhibitory properties of the pyrrolidine derivatives and might reflect additional steric requirements of the active center of the enzyme.

Conclusions

Chemoenzymatic methods using DHAP-dependent aldolases as biocatalysts for the key aldol addition step are both convenient and advantageous for the generation of configurational and functional collections of polyhydroxylated pyrrolidine compounds for bioactivity testing. FucA had restricted substrate tolerance for C-α linear *N*-Cbz-2-aminoaldehydes, whereas RhuA accepted all types of C-α substitutions selected. On the other hand, D-fructose-1,6-bisphos-

phate aldolase from rabbit muscle (RAMA) did not catalyze the aldol reactions with any of the selected aminoaldehydes. FucA catalyst was the most steroselective (i.e., *anti* (3*R*,4*R*) configuration of the stereogenic centers formed) catalyst, the stereochemical outcome of the reactions being controlled by the enzyme. RhuA was highly stereoselective (i.e., *syn* (3*R*,4*S*)) for the (*S*)-aminoaldehydes regardless of the C-α substitution, but non-selective with the (*R*)-aminoaldehydes giving mixtures of *anti/syn* adducts. Molecular models of selected RhuA–aldol adduct complexes revealed that the *anti* adducts modeled were lower in energy than the corresponding *syn* adducts. Given the similarity between the geometries of the complexes and the corresponding transition states, these models would suggest a kinetic preference that could explain the formation of larger proportions of *anti* adducts from aldehydes (*R*)-**2c** or (*R*)-**2d** and could provide an explanation to the temperature effects. Drawbacks of this approach are thus the acceptor substrate tolerance, occasionally lack of stereoselectivity, which in some instances depends on acceptor structure, or an unfavorable equilibrium position of the addition reaction. These might be overcome with both enzyme and medium engineering, aspects that are being currently under investigation in our lab.

Examination of the inhibitory properties of the compounds showed that they are good inhibitors of α-L-fucosidase (IC_{50} = 1–20 μM), moderate of α-L-rhamnosidase (IC_{50} = 7–150 μM) and weak of α-D-mannosidase (IC_{50} = 80–400 μM). The docking results obtained with α-L-fucosidase show a good correlation with the experimental activities, and indicate that small alkyl chains at C-5 position of the pyrrolidine are preferred for high affinity. We report for the first time a strong α-L-fucosidase inhibition for the 5-methyl substituted pyrrolidine with 2*R*,3*S*,4*R*,5*S* configuration, more than ≈30000-fold higher than for its 2*R*,3*R*,4*R*,5*R* diastereomer, revealing the great importance of the stereochemistry for the activity of these compounds. On the other hand, preliminary results obtained with an α-L-rhamnosidase model would suggest that larger C-5 alkyl substituents might interact more strongly with its active center. Finally, the results obtained for α-D-mannosidase are not conclusive for the compounds described in this work.

Experimental Section

Materials: D-Fructose-1,6-bisphosphate aldolase from rabbit muscle (RAMA; EC 4.1.2.13, crystallized, lyophilized powder, 19.5 U mg^{-1}) was from Fluka (Buchs, Switzerland). Rhamnulose-1-phosphate aldolase (RhuA; EC 4.1.2.19, suspension 100 U mL^{-1}) was kindly donated by Roche Diagnostics (Mannhein, Germany). L-Fuculose-1-phosphate aldolase (FucA, EC 4.1.2.17, lyophilized 500–800 U g^{-1} or as $(NH_4)_2SO_4$ suspension (25 U mL^{-1}) was from Departament d'Enginyeria Química of the Universitat Autònoma de Barcelona, produced from a recombinant *E. coli* (ATCC no 86984) and purified by affinity chromatography. Acid phosphatase (PA, EC 3.1.3.2, 5.3 U mg^{-1}) was from Sigma (St. Louis, USA). The precursor of dihydroxyacetone phosphate (DHAP), the dihydroxyacetone phosphate diethyl ketal dimer, was synthesized in our lab by using a procedure described by Jung et al.[68] with slight modifications. Aluminum oxide 90 active neutral was purchased from Merck. Celite-545 (particle size 26 μm, mean pore diameter 17000 nm, specific surface area BET method 2.19 $m^2 g^{-1}$) was obtained from Fluka. α-D-Glucosidase from baker's yeast, β-D-glucosidase from sweet almonds, β-D-galactosidase from bovine liver, α-D-mannosidase from jack bean, α-L-rhamnosidase (naranginase) from *Penicillium decumbens*, and α-L-fucosidase from bovine kidney and the corresponding substrates *p*-nitrophenyl-α-D-glucopyranoside, *p*-nitrophenyl-β-D-glucopyranoside, *p*-nitrophenyl-β-D-galactopyranoside, *p*-nitrophenyl-α-D-mannopyranoside, *p*-nitrophenyl-α-L-rhamnopyranoside, and *p*-nitrophenyl-α-L-fucopyranoside, respectively, were purchased from Sigma. Deionized water was used for preparative HPLC and Milli-Q-grade water for analytical HPLC. All other solvents used were of analytical grade.

NMR spectroscopy: ^{1}H (500.13 MHz) and ^{13}C (125.76 MHz) NMR spectra were recorded on an Avance 500 Bruker spectrometer equipped with a highly sensitive, cryogenically cooled, triple-resonance TCI probehead for samples dissolved in D_2O and CD_3OD. Full structural and stereochemical characterization of all compounds was performed with the aid of two dimensional COSY, NOESY, HSQC, and HMBC experiments as well as NOE data obtained from selective 1D NOESY experiments recorded with a mixing time of 500 ms. The relative orientation of hydroxyl groups was determined from the characteristic downfield/upfield effects observed for all H-1, H-2, H-3, H-7a proton chemical shift, as recently reported for other iminocyclitols.[24,25] As a general trend, strong downfield effects are observed for the most characteristic H-1, H-2, and H-3 protons when the corresponding vicinal hydroxyl groups were found in a relative *anti* position. ^{1}H and ^{13}C chemical shifts were calibrated to a DSS external reference.

Specific rotations: Measurements were made on a Perkin–Elmer Model 341 (Überlingen, Germany) polarimeter.

HPLC analyses: HPLC analyses were performed on a RP-HPLC cartridge, 250×4 mm filled with Lichrosphere 100, RP-18, 5 μm from Merck (Darmstadt, Germany). Samples (50 mg of the emulsion mixture or 50 μL of the reaction in DMF/water 1:4) were withdrawn from the aldol reaction, dissolved in MeOH (1 mL) to stop the reaction and analyzed by HPLC. The solvent system used was the following: solvent A: H_2O 0.1% (v/v) trifluoroacetic acid (TFA); solvent B: ACN/H_2O 4:1 0.095% (v/v) TFA, gradient elution from 30 to 90% B over 30 min, flow rate 1 mL min^{-1}, detection 215 nm.

General procedure for the synthesis of (*S*)- or (*R*)-*N*-benzyloxycarbonylaminoaldehydes: Cbz-OSu (50 mmol) in dioxane/water 4:1 (10–50 mL) was added dropwise to a solution of (*S*) or (*R*)-aminoalcohol (50 mmol) in dioxane/water 4:1 (100 mL) at 25 °C. After stirring for 24 h, the mixture was evaporated to dryness under reduced pressure. The residue was dissolved with ethyl acetate (150 mL) and washed successively with citric acid 5% w/v (3×50 mL), $NaHCO_3$ 10% w/v (3×50 mL), and brine (2×50 mL). After drying over Na_2SO_4, the organic layer was evaporated under reduced pressure affording white solids of (*S*)- and (*R*)-*N*-Cbz-aminoalcohols (mean yield: 85% yield; 98% purity by HPLC). NMR spectrum analysis of the residue showed only one product. Oxidation of (*R*)- or (*S*)-*N*-Cbz-aminoalcohols (25 mmol) was efficiently carried out by a procedure described by Ocejo et al.[69]

(*S*)-1-Oxobutane-2-benzylcarbamate ((*S*)-2a): Pale yellow oil; yield: 2.5 g, 96%; 99.9% purity by HPLC; $[\alpha]_D^{20} = +18.0°$ (c = 0.9 in CH_2Cl_2); ^{1}HNMR: (300 MHz, $CDCl_3$): δ = 9.6 (s, 1H; CHO), 7.4 (m, 5H; Ph), 5.4 (br s, 1H; NH), 5.1 (s, 2H; PhCH_2O), 4.3 (dd, J = 6.7, 12.8 Hz, 1H; CHCHO), 2.0, 1.7 (m, 2H; CH_3CH_2), 1.0 ppm (t, J = 7.9 Hz, 3H; CH_3); ^{13}CNMR: (75 MHz, $CDCl_3$): δ = 199.1 (CHO), 155.0 (OCONH), 136.0 (C ar), 128.5 (C ar), 128.2 (C ar), 127.9 (C ar), 67.0 (PhCH_2O), 60.3 (CH), 22.2 (CH_3CH_2), 9.2 ppm (CH_3CH_2).

(*R*)-1-Oxobutane-2-benzylcarbamate ((*R*)-2a): Pale yellow oil; yield: 2 g, 97%; 99.9% purity by HPLC; $[\alpha]_D^{20} = -25.0°$ (c = 1.0 in CH_2Cl_2); ^{1}HNMR: (300 MHz, $CDCl_3$): δ = 9.6 (s, 1H; CHO), 7.4 (m, 5H; Ph), 5.4 (br s, 1H; NH), 5.1 (s, 2H; PhCH_2O), 4.3 (dd, J = 6.7, 12.8 Hz, 1H; CHCHO), 2.0, 1.7 (m, 2H; CH_3CH_2), 1.0 ppm (t, J = 7.1 Hz, 3H; CH_3); ^{13}CNMR: (75 MHz, $CDCl_3$): δ = 199.1 (CHO), 155.0 (OCONH), 136.0 (C ar), 128.5 (C ar), 128.2 (C ar), 127.9 (C ar), 67.0 (PhCH_2O), 60.3 (CH), 22.2 (CH_3CH_2), 9.2 ppm (CH_3CH_2).

(*S*)-1-Oxopentane-2-benzylcarbamate ((*S*)-2b): Oil; yield: 2.7 g, 98%; 99.9% purity by HPLC; $[\alpha]_D^{20}=+13°$ ($c=0.8$ in CH_2Cl_2); ^{1}HNMR: (300 MHz, $CDCl_3$): $\delta=9.6$ (s, 1H; CHO), 7.3 (m, 5H; Ph), 5.4 (brs, 1H; NH), 5.1 (s, 2H; PhCH_2O), 4.3 (dd, $J=6.7$, 12.8 Hz, 1H; NHCH), 1.8, 1.6 (m, 2H; CHCH_2), 1.4 (m, 2H; CH_2CH_3), 0.9 ppm (t, $J=7.5$ Hz, 3H; CH_2CH_3); ^{13}CNMR: (75 MHz, $CDCl_3$): $\delta=199.4$ (CHO), 156.0 (OCONH), 136.0 (C ar), 128.5 (C ar), 128.2 (C ar), 128.0 (C ar), 67.0 (PhCH_2O), 60.0 (CH), 31.1 (CHCH_2), 18.3 (CH_2CH_3), 13.7 ppm (CH_3).

(*R*)-1-Oxopentane-2-benzylcarbamate ((*R*)-2b): Oil; yield: 2.6 g, 97%; 99.9% purity by HPLC; $[\alpha]_D^{20}=-15.0°$ ($c=1.0$ in CH_2Cl_2); ^{1}HNMR: (300 MHz, $CDCl_3$): $\delta=9.6$ (s, 1H; CHO), 7.3 (m, 5H; Ph), 5.4 (brs, 1H; NH), 5.1 (s, 2H; PhCH_2O), 4.3 (dd, $J=6.7$, 12.8 Hz, 1H; NHCH), 1.8, 1.6 (m, 2H; CHCH_2), 1.4 (m, 2H; CH_2CH_3), 0.9 ppm (t, $J=7.5$ Hz, 3H; CH_2CH_3); ^{13}CNMR: (75 MHz, $CDCl_3$): $\delta=199.4$ (CHO), 156.0 (OCONH), 136.0 (C ar), 128.5 (C ar), 128.2 (C ar), 128.0 (C ar), 67.0 (PhCH_2O), 60.0 (CH), 31.1 (CHCH_2), 18.3 (CH_2CH_3), 13.7 ppm (CH_3).

(*S*)-1-Oxohexane-2-benzylcarbamate ((*S*)-2c): Oil; yield: 3.1 g, 97%; 99.9% purity by HPLC; $[\alpha]_D^{20}=-8.7°$ ($c=0.5$ in MeOH); ^{1}HNMR: (300 MHz, $CDCl_3$): $\delta=9.5$ (s, 1H; CHO), 7.3 (m, 5H; Ph), 5.6 (brs, 1H; NH), 5.1 (s, 2H; PhCH_2O), 4.2 (m, 1H; CH), 1.8 (m, 1H; CHCH_2), 1.6 (m, 1H; CHCH_2), 1.3 (m, 4H; CH$CH_2CH_2CH_3$), 0.9 ppm (t, $J=6.9$ Hz, 3H; CH_3); ^{13}CNMR: (75 MHz, $CDCl_3$): $\delta=199.7$ (CHO), 156.1 (OCONH), 136.1 (C ar), 128.4 (C ar), 128.1 (C ar), 128.0 (C ar), 66.9 (PhCH_2O), 60.1 (CHCHO), 28.6 (CHCH_2), 27.1 (CHCH$_2CH_2$), 22.3 (CH_3CH_2), 13.7 ppm (CH_3).

(*R*)-1-Oxohexane-2-benzylcarbamate ((*R*)-2c): Oil; yield: 3.1 g, 97%; 99.9% purity by HPLC; $[\alpha]_D^{20}=+8.2°$ ($c=0.7$ in MeOH); ^{1}HNMR: (300 MHz, $CDCl_3$): $\delta=9.5$ (s, 1H; CHO), 7.3 (m, 5H; Ph), 5.6 (brs, 1H; NH), 5.1 (s, 2H; PhCH_2O), 4.2 (m, 1H; CH), 1.8 (m, 1H; CHCH_2), 1.6 (m, 1H; CHCH_2), 1.3 (m, 4H; CH$CH_2CH_2CH_3$), 0.9 ppm (t, $J=6.9$ Hz, 3H; CH_3); ^{13}CNMR: (75 MHz, $CDCl_3$): $\delta=199.7$ (CHO), 156.1 (OCONH), 136.1 (C ar), 128.4 (C ar), 128.1 (C ar), 128.0 (C ar), 66.9 (PhCH_2O), 60.1 (CHCHO), 28.6 (CHCH_2), 27.1 (CHCH$_2CH_2$), 22.3 (CH_3CH_2), 13.7 ppm (CH_3).

(*S*)-3-Methyl-1-oxobutane-2-benzylcarbamate ((*S*)-2d): Pale yellow oil; yield: 4.2 g, 95%; 99.9% purity by HPLC; $[\alpha]_D^{20}=+8.2°$ ($c=1.7$ in MeOH); ^{1}HNMR: (300 MHz, $CDCl_3$): $\delta=9.6$ (s, 1H; CHO), 7.4 (m, 5H; Ph), 5.4 (brs 1H; NH), 5.1 (s, 2H; PhCH_2O), 4.3 (m, 1H; CHCHO), 2.3 (m, 1H; $CH(CH_3)_2$), 1.0 (d, $J=6.9$ Hz, 3H; CH_3), 0.9 ppm (d, $J=7.0$ Hz, 3H; CH_3); ^{13}CNMR: (75 MHz, $CDCl_3$): $\delta=199.7$ (CHO), 156.3 (OCONH), 136.1 (C ar), 128.5 (C ar), 128.2 (C ar), 128.0 (C ar), 67.0 (PhCH_2O), 64.9 (CHCHO), 29.0 ($CH(CH_3)_2$), 18.9, 17.4 ppm ((CH_3)$_2$).

(*R*)-3-Methyl-1-oxobutane-2-benzylcarbamate ((*R*)-2d): Pale yellow oil; yield: 4 g, 96%; 99.9% purity by HPLC; $[\alpha]_D^{20}=-8.5°$ ($c=1.3$ in MeOH); ^{1}HNMR: (300 MHz, $CDCl_3$): $\delta=9.6$ (s, 1H; CHO), 7.4 (m, 5H; Ph), 5.4 (brs 1H; NH), 5.1 (s, 2H; PhCH_2O), 4.3 (m, 1H; CHCHO), 2.3 (m, 1H; $CH(CH_3)_2$), 1.0 (d, $J=6.9$ Hz, 3H; CH_3), 0.9 ppm (d, $J=7.0$ Hz, 3H; CH_3); ^{13}CNMR: (75 MHz, $CDCl_3$): $\delta=199.7$ (CHO), 156.3 (OCONH), 136.1 (C ar), 128.5 (C ar), 128.2 (C ar), 128.0 (C ar), 67.0 (PhCH_2O), 64.9 (CHCHO), 29.0 ($CH(CH_3)_2$), 18.9, 17.4 ppm ((CH_3)$_2$).

(2*S*,3*S*)-3-Methyl-1-oxopentane-2-benzylcarbamate ((*S*)-2e): Pale yellow oil; yield: 2.4 g, 95%; 99.9% purity by HPLC; $[\alpha]_D^{20}=+5.8°$ ($c=1.2$ in MeOH); ^{1}HNMR: (300 MHz, $CDCl_3$): $\delta=9.7$ (s, 1H; CHO), 7.4 (m, 5H; Ph), 5.4 (brd, $J=6.8$ Hz, 1H; NH), 4.4 (m, 1H; CHCHO), 1.5, 1.3 (m, 2H; CH_2CH_3), 1.2 (m, 1H; CHCH$_3$), 1.0 ppm (m, 6H; CH_3); ^{13}CNMR: (75 MHz, $CDCl_3$): $\delta=200.0$ (CHO), 156.2 (OCONH), 136.1 (C ar), 128.5 (C ar), 128.2 (C ar), 128.1 (C ar), 67.0 (PhCH_2O), 64.6 (CHCHO), 36.3 (CHCH$_3$), 25.2 (CH_2CH_3), 15.5 (CHCH_3), 11.9 ppm (CH$_2CH_3$).

(*S*)-4-Methyl-1-oxopentane-2-benzylcarbamate ((*S*)-2f): Pale yellow oil; yield: 4.1 g, 97%; 99.9% purity by HPLC; $[\alpha]_D^{20}=-33.5°$ ($c=1.1$ in MeOH); ^{1}HNMR: (300 MHz, $CDCl_3$): $\delta=9.6$ (s, 1H; CHO), 7.4 (m, 5H; Ph), 5.2 (brs 1H; NH), 5.1 (s, 2H; Ph$CH2$O), 4.3 (m, 1H; CHCHO), 1.7 (m, 2H; CH$_2$), 1.4 (m, 1H; $CH(CH_3)_2$), 1.0 ppm (m, 6H; CH_3); ^{13}CNMR: (75 MHz, $CDCl_3$): $\delta=199.6$ (CHO), 158.3 (OCONH), 166.7 (C ar), 128.5 (C ar), 128.2 (C ar), 128.0 (C ar), 67.1 (PhCH_2O), 58.7 (CHCHO), 38.0 (CH$_2$), 23.0 ($CH(CH_3)_2$), 24.5, 22.0 ppm (CH_3).

(*R*)-4-Methyl-1-oxopentane-2-benzylcarbamate ((*R*)-2f): Pale yellow oil; yield: 4.1 g, 97%; 99.9% purity by HPLC; $[\alpha]_D^{20}=+30.8°$ ($c=1.1$ in MeOH); ^{1}HNMR: (300 MHz, $CDCl_3$): $\delta=9.6$ (s, 1H; CHO), 7.4 (m, 5H; Ph), 5.2 (brs 1H; NH), 5.1 (s, 2H; PhCH_2O), 4.3 (m, 1H; CHCHO), 1.7 (m, 2H; CH$_2$), 1.4 (m, 1H; $CH(CH_3)_2$), 1.0 ppm (m, 6H; CH_3); ^{13}CNMR: (75 MHz, $CDCl_3$): $\delta=199.6$ (CHO), 158.3 (OCONH), 166.7 (C ar), 128.5 (C ar), 128.2 (C ar), 128.0 (C ar), 67.1 (PhCH_2O), 58.7 (CHCHO), 38.0 (CH$_2$), 23.0 ($CH(CH_3)_2$), 24.5, 22.0 ppm (CH_3).

(*S*)-1-Oxo-3-phenylpropan-2-benzylcarbamate ((*S*)-2g): Oil; yield: 3.4 g, 97%; 99.9% purity by HPLC; $[\alpha]_D^{20}=-53.0°$ ($c=0.6$ in DMF); ^{1}HNMR: (300 MHz, $CDCl_3$): $\delta=9.7$ (s, 1H; CHO), 7.4 (m, 10H; Ph), 5.4 (d, $J=6.1$ Hz, 1H; NH), 5.1 (s, 1H; PhCH_2O), 4.5 (dd, $J=6.8$, 13.5 Hz, 1H; PhCH$_2CH$), 3.2 ppm (d, $J=6.5$ Hz, 2H; PhCH_2CH); ^{13}CNMR: (75 MHz, $CDCl_3$): $\delta=199.2$ (CHO), 155.2 (OCONH), 136.3 (C ar), 135.7 (C ar), 129.6 (C ar), 129.1 (C ar), 128.9 (C ar), 128.8 (C ar), 128.8 (C ar), 128.8 (C ar), 67.4 (CH), 61.4 (PhCH_2O), 35.6 ppm (PhCH_2CH).

2-Methyl-1-oxopropane-2-benzylcarbamate (2h): Oil; yield: 3.6 g, 94%; 99.9% purity by HPLC; ^{1}HNMR: (300 MHz, $CDCl_3$): $\delta=9.4$ (s, 1H; CHO), 7.3 (m, 5H; Ph), 5.4 (brs 1H; NH), 1.4 ppm (s, 6H; CH_3); ^{13}CNMR: (75 MHz, $CDCl_3$): $\delta=200.3$ (CHO), 171.1 (OCONH), 155.1 (C ar), 128.5 (C ar), 128.2 (C ar), 128.1 (C ar), 66.8 (PhCH_2O), 59.4 (CCHO), 21.7 ppm (CH_3).

Enzymatic aldol condensation: Analytical scale reactions (2.5 mL total volume) were conducted in 10 mL test tubes with screw caps at [DHAP] = 50–100 mM, [*N*-Cbz-aminoaldehyde] = 85–170 mM depending on the results obtained at analytical scale. Reactions at preparative scale (15–20 mL total volume) were performed in 50 mL test tubes with screw caps. The other variables were scaled up in proportion to the final volume. As example, the procedure followed is described below.

Enzymatic aldol condensations in emulsions: (*S*)- or (*R*)-*N*-Cbz-aminoaldehyde (0.13–4.8 mmol, 1.7 equiv per mol DHAP), the oil (6% w/w), and the surfactant (4% w/w) were mixed with a vortex mixer. Then, the DHAP solution (volume corresponding to 90% w/w of the mixture, 0.075–3 mmol) at pH 6.9, freshly prepared as described by Effenberger et al.,[70] was added dropwise while stirring at 25 °C or 4 °C depending on the experiment with a vortex mixer. The reactions were started by adding RAMA (8 U mL^{-1} reaction mixture), RhuA (2 U mL^{-1} reaction mixture), or FucA (8 U mL^{-1} reaction mixture) and mixed again. The test tubes were placed on a horizontal shaking bath (100 rpm) at constant temperature (4 or 25 °C depending on the experiment). The reactions were followed by HPLC, as indicated above, until the peak of the product reached a maximum.

Enzymatic aldol condensations in mixtures water/dimethylformamide 4:1: (*S*)- or (*R*)-*N*-Cbz-aminoaldehyde (0.13–4.8 mmol, 1.7 equiv per mol DHAP) was dissolved in DMF (the amount corresponding to 20% v/v of the total). Then, the DHAP solution (volume corresponding to 80% v/v of the total, 0.075–3 mmol) at pH 6.9, freshly prepared as described above was added dropwise while stirring at 25 or 4 °C, depending on the experiment, with a vortex mixer. Finally, RAMA (8 U mL^{-1} reaction mixture), RhuA (2 U mL^{-1} reaction mixture), or FucA (8 U mL^{-1} reaction mixture) was added and mixed again. The rest of the experimental procedure was identical to that described for the reaction in emulsions.

The enzymatic reactions were stopped by addition of MeOH (1.5xreaction volume). Then, the methanol was evaporated and the aqueous solution washed with ethyl acetate to remove the unreacted *N*-protected aminoaldehyde. The aqueous layer was collected, the remaining ethyl acetate removed under reduced pressure, and lyophilized. The solid obtained was dissolved in plain water (ca. 10–20 mL) and the pH was adjusted to 5.5 either with TFA or with HCl. To this solution, acid phosphatase (5.3 U mmol^{-1} phosphated adduct) was added. The reaction was followed by HPLC until no starting material was detected. Further phosphatase units were added, if necessary, to direct the reaction to completion. Then, the reaction mixture was filtered through a 0.45 μm cellulose membrane filter. The filtrate was loaded onto a Perkin–Elmer semipreparative 250×25 mm column, filled with C18 (10 μm) and eluted with a gradient of CH_3CN (0 to 48% over 30 min) in plain water. Pure fractions were pooled and lyophilized.

Removal of Cbz group and reductive amination: The aldol adduct obtained (0.011–0.24 mmol) was dissolved in ethanol (5–10 mL) followed with the addition of plain water (20–45 mL). Pd/C (200 mg) was added to this solution. The reaction mixture was shaken under hydrogen gas (50 psi) overnight at room temperature. After removal of the catalyst by filtration through neutralized and deactivated aluminum, the pH of the filtrate was adjusted to pH 5.5 with HCl, and the solvent was evaporated under reduced pressure and then lyophilized. Characterization of the products from the lyophilisates was accomplished by NMR spectroscopy.

Physical, ^{1}H and ^{13}C NMR data of the compounds synthesized: For the sake of clarity in the systematic nomenclature, we always assign the hydroxymethyl group at position C-2. For detailed assignments of H and C in the spectra see Supporting Information. Entry numbers correspond to the entries in Table 1.

Entry 1—(2*S*,3*S*,4*S*,5*S*)-2-(hydroxymethyl)pyrrolidine-5-ethyl-3,4-diol (4a): Yield: 0.222 mmol, 44 mg, 63%; $[\alpha]_D^{20} = -36.7°$ ($c = 1$ in MeOH); ^{1}H NMR (500.13 MHz, D_2O): $\delta = 4.03$ (t, $^3J(H,H) = 7.3$ Hz, 1H), 3.94 (m, 1H), 3.90 (A of AB system, $^3J(H,H) = 12.6$, 3.7 Hz, 1H), 3.83 (B of AB system, $^3J(H,H) = 12.7$, 6.1 Hz, 1H), 3.53 (m, 1H), 3.33 (m, 1H), 1.91 (m, 1H), 1.75 (m, 1H), 1.03 ppm (t, $^3J(H,H) = 7.5$ Hz, 3H). ^{13}C NMR (101 MHz, D_2O): $\delta = 80.6$ (C4), 76.9 (C3), 65.7 (C5), 64.8 (C2), 60.6 (C6), 26.2 (C7), 12.4 ppm (C8); ESI-TOF: m/z calcd for $[M+H]^+$ $C_7H_{16}NO_3$: 162.1130; found: 162.1125.

Entry 2—(2*R*,3*S*,4*R*,5*S*)-2-(Hydroxymethyl)pyrrolidine-5-ethyl-3,4-diol (4b; 86%), (2*S*,3*S*,4*S*,5*S*)-2-(hydroxymethyl)pyrrolidine-5-ethyl-3,4-diol (4a; 10%), and (2*R*,3*S*,4*R*,5*S*)-2-(hydroxymethyl)pyrrolidine-5-ethyl-3,4-diol (4c; 4%): Overall yield: 0.101 mmol, 20 mg, 28%; $[\alpha]_D^{20} = +14.3°$ ($c = 0.9$ in MeOH).

*Data for **4b***: ^{1}H NMR (500 MHz, D_2O): $\delta = 4.23$ (m, 1H), 4.22 (m, 1H), 3.91 (A of AB system, $^3J(H,H) = 12.6$, 3.4 Hz, 1H), 3.78 (A of AB system, $^3J(H,H) = 12.6$, 6.0 Hz, 1H), 3.55 (m, 1H), 3.50 (dt, $^3J(H,H) = 7.5$, 1.5 Hz, 1H), 1.96–1.66 (m, 2H), 0.95 ppm (t, $^3J(H,H) = 7.5$ Hz, 3H). ^{13}C NMR (101 MHz, D_2O): $\delta = 74.1$ (C4), 73.1 (C3), 65.9 (C5), 64.2(C2), 61.0 (C6), 22.2 (C7), 12.4 ppm (C8). ESI-TOF: m/z calcd for $[M+H]^+$ $C_7H_{16}NO_3$: 162.1130; found: 162.1125.

*Data for **4a***: See ^{1}H and ^{13}C NMR of entry 1.

*Data for **4c***: The main ^{1}H and ^{13}C NMR chemical shifts are similar to those of entry 6 (**4j**). ESI-TOF: m/z calcd for $[M+H]^+$ $C_7H_{16}NO_3$: 162.1130; found: 162.1127.

Entry 3—(2*S*,3*S*,4*S*,5*R*)-2-(hydroxymethyl)pyrrolidine-5-ethyl-3,4-diol (4d; 48%), (2*R*,3*S*,4*R*,5*R*)-2-(hydroxymethyl)pyrrolidine-5-ethyl-3,4-diol (4e; 30%), *N*-ethyl-(2*S*,3*S*,4*S*,5*R*)-2-(hydroxymethyl)pyrrolidine-5-ethyl-3,4-diol (4f; 11%), and *N*-ethyl-(2*R*,3*S*,4*R*,5*R*)-2-(hydroxymethyl)pyrrolidine-5-ethyl-3,4-diol (4g; 11%): Overall yield: 0.152 mmol, 30 mg, 61%; $[\alpha]_D^{20} = -12.4°$ ($c = 1.0$ MeOH).

*Data for **4d***: ^{1}H NMR (500 MHz, D_2O): $\delta = 4.15$ (m, 1H), 4.04 (m, 1H), 3.84 (A of AB system, $^3J(H,H) = 12.0$, 8.6 Hz, 1H), 3.77 (B of AB system, $J = 12.0$, 8.9 Hz, 1H), 3.72 (m, 1H), 3.64 (m, 1H), 1.78 (m, 2H), 1.01 ppm (t, $^3J(H,H) = 7.5$ Hz, 3H); ^{13}C NMR (101 MHz, D_2O): $\delta = 78.8$ (C3), 77.6 (C4), 70.2 (C2), 67.1 (C5), 62.4 (C6), 21.2 (C7), 12.7 ppm (C8). ESI-TOF: m/z calcd for $[M+H]^+$ $C_7H_{16}NO_3$: 162.1130; found: 162.1125.

*Data for **4e***: The main ^{1}H and ^{13}C NMR chemical shifts are listed in entry 4. ESI-TOF: m/z calcd for $[M+H]^+$ $C_7H_{16}NO_3$: 162.1130; found: 162.1125.

*Data for **4f***: ^{1}H NMR (500 MHz, D_2O): $\delta = 4.30$ (d, $^3J(H,H) = 2.8$ Hz, 1H), 4.19 (s, 1H), 3.96 (d, $^3J(H,H) = 1.2$ Hz, 1H), 3.95 (s, 1H), 3.70 (m, 1H), 3.61 (t, $^3J(H,H) = 6.5$ Hz, 1H), 3.53 (A of AB system, $^3J(H,H) = 14.6$, 7.4 Hz, 1H), 3.31 (B of AB system, $^3J(H,H) = 14.5$, 7.3 Hz, 1H), 1.87 (m, 1H), 1.35 (t, $^3J(H,H) = 7.3$ Hz, 1H), 1.04 ppm (t, $^3J(H,H) = 7.5$ Hz, 1H); ^{13}C NMR (101 MHz, D_2O): $\delta = 77.4$ (C3), 75.9 (C4), 76.0 (C2), 72.0 (C5), 61.7 (C6), 50.7 (C9,9′), 19.3 (C7), 12.3 (C8), 10.3 ppm (C10). ESI-TOF: m/z calcd for $[M+H]^+$ $C_9H_{20}NO_3$: 190.1437; found: 190.1432.

*Data for **4g** (free base)*: ^{1}H NMR (500 MHz, D_2O): $\delta = 4.21$ (m, 1H), 3.95 (m, 1H), 3.85 (A of an AB system, $^3J(H,H) = 11.5$, 6.4 Hz, 1H), 3.74 (B of an AB system, 1H overlapped), 3.51 (m, 1H), 3.12 (m, 1H), 2.81 (m, 1H), 2.73 (m, 1H), 1.74 (m, 1H), 1.57 (m, 1H), 1.15 (t, $^3J(H,H) = 7.2$ Hz, 1H), 0.97 ppm (m, 3H overlapped); ^{13}C NMR (101 MHz, D_2O): $\delta = 75.1$ (C4), 72.0 (C3), 72.4 (C5), 61.0 (C2), 60.1 (C6), 52.9 (C9,9′), 24.9 (C7), 11.5 (C10), 11.3 ppm (C8). ESI-TOF: m/z calcd for $[M+H]^+$ $C_9H_{20}NO_3$: 190.1437; found: 190.1433.

Entry 4—(2*R*,3*S*,4*R*,5*R*)-2-(hydroxymethyl)pyrrolidine-5-ethyl-3,4-diol (4e): Yield: 0.137 mmol, 27 mg, 20%; $[\alpha]_D^{20} = +47.6°$ ($c = 0.8$ in MeOH); ^{1}H NMR (500 MHz, D_2O): $\delta = 4.28$ (t, $J = 3.5$ Hz, 1H), 4.09 (dd, $^3J(H,H) = 9.3$, 3.7 Hz, 1H), 3.96 (A of AB system, $^3J(H,H) = 11.9$, 4.9 Hz, 1H), 3.85 (A of AB system, $^3J(H,H) = 11.9$, 8.4 Hz, 1H), 3.74 (m, 1H), 3.42 (dt, $^3J(H,H) = 9.3$, 5.2 Hz, 1H), 1.87 (m, 1H), 1.73 (m, 1H), 1.02 ppm (t, $^3J(H,H) = 7.5$ Hz, 3H); ^{13}C NMR (101 MHz, D_2O): $\delta = 77.8$ (C4), 72.9 (C3), 64.8 (C2), 64.1 (C5), 60.4 (C6), 26.1 (C7), 12.8 ppm (C8); ESI-TOF: m/z calcd for $[M+H]^+$ $C_7H_{16}NO_3$: 162.1130; found: 162.1126.

Entry 5—(2*S*,3*S*,4*S*,5*S*)-2-(hydroxymethyl)pyrrolidine-5-propyl-3,4-diol (4h): Yield: 0.708 mmol, 150 mg, 67%; $[\alpha]_D^{20} = -40.6°$ ($c = 1.0$ in MeOH); ^{1}H NMR (400 MHz, D_2O): $\delta = 4.01$ (t, $^3J(H,H) = 7.2$ Hz, 1H), 3.91 (m, 1H), 3.86 (A of AB system, 1H), 3.81 (B of AB system, $^3J(H,H) = 12.7$, 5. 9 Hz, 1H), 3.51 (m, 1H), 3.38 (m, 1H), 1.82 (m, 1H), 1.70 (m, 1H), 1.41 (m, 2H), 0.90 ppm (t, $^3J(H,H) = 7.3$ Hz, 3H); ^{13}C NMR (101 MHz, D_2O): $\delta = 80.8$ (C4), 76.9 (C3), 64.8 (C5), 64.0 (C2), 60.6 (C6), 34.9 (C7), 21.4 (C8), 15.6 ppm (C9); ESI-TOF: m/z calcd for $[M+H]^+$ $C_8H_{18}NO_3$: 176.1287; found: 176.1281.

Entry 6—(2*S*,3*S*,4*R*,5*S*)-2-(hydroxymethyl)pyrrolidine-5-propyl-3,4-diol (4i; 86%), (2*S*,3*S*,4*S*,5*S*)-2-(hydroxymethyl)pyrrolidine-5-propyl-3,4-diol (4h; 4%), and (2*R*,3*S*,4*R*,5*S*)-2-(hydroxymethyl)pyrrolidine-5-propyl-3,4-diol (4j; 10%): Overall yield: 0.103 mmol, 22 mg, 21%; $[\alpha]_D^{20} = -28.3°$ ($c = 0.3$ in MeOH).

*Data for **4i***: ^{1}H NMR (500 MHz, D_2O): $\delta = 4.28$ (m, 1H), 4.27 (s, 1H), 3.96 (A of AB system, $^3J(H,H) = 12.6$, 3.5 Hz, 1H), 3.83 (B of AB system, $^3J(H,H) = 12.6$, 6.1 Hz, 1H), 3.64 (t, $^3J(H,H) = 7.4$ Hz, 1H), 3.60 (m, 1H), 1.73 (m, 1H), 1.42 (m, 2H), 0.96 ppm (t, $^3J(H,H) = 7.2$ Hz, 3H). ^{13}C NMR (101 MHz, D_2O): $\delta = 74.1$ (C4), 73.3 (C3), 64.2 (C5), 64.2 (C2), 61.1 (C6), 30.8 (C7), 21.4 (C8), 15.7 ppm (C9). ESI-TOF: m/z calcd for $[M+H]^+$ $C_8H_{18}NO_3$: 176.1287; found: 176.1281.

*Data for **4h***: See the main ^{1}H and ^{13}C NMR chemical shifts listed for entry 5.

*Data for **4j***: ^{1}H NMR (500 MHz, D_2O δ ppm 4.53 (dd, $^3J(H,H) = 7.6$ Hz, 1H), 4.33 (t, $^3J(H,H) = 4.4$ Hz, 1H), 3.94 (A of AB system, $^3J(H,H) = 12.1$, 4.2 Hz, 1H), 3.85 (B of AB system, $^3J(H,H) = 12.1$, 8.5 Hz, 1H), 3.78 (m, 1H), 3.54 (m, 1H), 1.81 (m, 1H), 1.71 (m, 1H), 1.41 (m, 1H), 0.95 ppm (t, $^3J(H,H) = 7.4$ Hz, 1H); ^{13}C NMR (101 MHz, D_2O): $\delta = 72.7$ (C4), 72.7 (C3), 62.9 (C5), 62.9 (C2), 60.2 (C6), 30.1 (C7), 21.1 (C8), 15.3 ppm (C9). ESI-TOF: m/z calcd for $[M+H]^+$ $C_8H_{18}NO_3$: 176.1287; found: 176.1284.

Entry 7—(2*S*,3*S*,4*S*,5*R*)-2-(hydroxymethyl)pyrrolidine-5-propyl-3,4-diol (4k;44%), (2*R*,3*S*,4*R*,5*R*)-2-(hydroxymethyl)pyrrolidine-5-propyl-3,4-diol (4l; 34%), *N*-ethyl-(2*S*,3*S*,4*S*,5*R*)-2-(hydroxymethyl)pyrrolidine-5-propyl-3,4-diol (4m; 11%), and *N*-ethyl-(2*R*,3*S*,4*R*,5*R*)-2-(hydroxymethyl)pyrrolidine-5-propyl-3,4-diol (4n; 10%): Overall yield: 0.180 mmol, 38 mg, 78%; $[\alpha]_D^{20} = +15.7°$ ($c = 1.0$ in MeOH).

*Data for **4k***: ^{1}H NMR (500 MHz, D_2O): $\delta = 4.14$ (br d, 1H), 4.06 (m, 1H), 3.97 (A of AB system, $^3J(H,H) = 12.0$, 8.5 Hz, 1H), 3.86 (B of AB system, $^3J(H,H) = 7.3$, 2.8 Hz, 1H), 3.78 (dd, $^3J(H,H) = 12.1$, 8.9 Hz, 1H), 3.55 (m, 1H), 1.75 (m, 2H), 1.43 (m, 2H), 0.94 ppm (m, 3H). ^{13}C NMR (101 MHz, D_2O): $\delta = 78.8$ (C3), 78.0 (C4), 72.2 (C2), 65.3 (C5), 63.0 (C6), 29.7 (C7), 21.8 (C8), 15.8 ppm (C9).

*Data for **4l***: See the ^{1}H and ^{13}C NMR chemical shifts listed in entry 8.

*Data for **4m***: The main ^{1}H and ^{13}C NMR chemical shifts are coincident to those for **4f**.

*Data for **4n***: The main ^{1}H and ^{13}C NMR chemical shifts are coincident to those for **4g**.

Entry 8—(2*R*,3*S*,4*R*,5*R*)-2-(hydroxymethyl)pyrrolidine-5-propyl-3,4-diol (4l): Yield: 0.136 mmol, 29 mg, 28%; $[\alpha]_D^{20} = +62.3°$ ($c = 1.0$ in MeOH); ^{1}H NMR (500 MHz, D_2O): $\delta = 4.28$ (t, $J = 3.4$ Hz, 1H), 4.08 (dd, $^3J(H,H) = 9.3$, 3.8 Hz, 1H), 3.96 (A of AB system, $^3J(H,H) = 12.1$, 5.0 Hz, 1H), 3.85 (B of AB system, $^3J(H,H) = 12.1$, 8.4 Hz, 1H), 3.75 (m, 1H),

3.50 (dt, ^3J(H,H) = 9.3, 5.1 Hz, 1H), 1.80 (m, 1H), 1.69 (m, 1H), 1.44 (m, 2H), 0.93 ppm (t, ^3J(H,H) = 7.3 Hz, 3H); ^{13}C NMR (101 MHz, D_2O): δ = 78.0 (C4), 72.9 (C3), 64.1 (C2), 63.0 (C5), 60.3 (C6), 34.9 (C7), 21.8 (C8), 15.6 ppm (C9); ESI-TOF: calcd for $[M+H]^+$ $C_8H_{18}NO_3$: 176.1287; found: 176.1282.

Entry 9—(2*S*,3*S*,4*S*,5*S*)-2-(hydroxymethyl)pyrrolidine-5-butyl-3,4-diol (4o; 93%) and (2*S*,3*S*,4*R*,5*S*)-2-(hydroxymethyl)pyrrolidine-5-butyl-3,4-diol (4p; 7%): Overall yield: 0.155 mmol, 35 mg, 62%; $[\alpha]_D^{20} = -27.1$ (c = 0.9 in MeOH).

Data for **4o**: ^{1}H NMR (500 MHz, D_2O): δ = 4.02 (t, ^3J(H,H) = 6.9 Hz, 1H), 3.93 (m, 1H), 3.90 (A of AB system, ^3J(H,H) = 12.6, 3.8 Hz, 1H), 3.83 (B of AB system, ^3J(H,H) = 12.6, 6.1 Hz, 1H), 3.53 (m, 1H), 3.38 (m, 1H), 1.86 (m, 1H), 1.72 (m, 1H), 1.35 (m, 4H), 0.86 ppm (t, ^3J(H,H) = 7.2 Hz, 3H); ^{13}C NMR (101 MHz, D_2O): δ = 80.8 (C4), 77.0 (C5), 64.8 (C2), 64.2 (C5), 60.6 (C6), 32.5 (C7), 30.0 (C8), 24.3 (C9), 15.7 ppm (C10); ESI-TOF: m/z calcd for $[M+H]^+$ $C_9H_{20}NO_3$: 190.1443; found: 190.1437.

Data for **4p**: The ^{1}H and ^{13}C NMR chemical shifts listed in entry 10.

Entry 10—(2*S*,3*S*,4*R*,5*S*)-2-(hydroxymethyl)pyrrolidine-5-butyl-3,4-diol (4p; 80%), (2*S*,3*S*,4*S*,5*S*)-2-(hydroxymethyl)pyrrolidine-5-butyl-3,4-diol (4o; 10%), and (2*R*,3*S*,4*R*,5*S*)-2-(hydroxymethyl)pyrrolidine-5-butyl-3,4-diol (4q; 10%): Overall yield: 0.088 mmol, 20 mg, 18%; $[\alpha]_D^{20} = -28.3°$ (c = 0.3 in MeOH).

Data for **4p**: ^{1}H NMR (500 MHz, D_2O): δ = 4.24 (m, 1H), 4.22 (m, 1H), 3.92 (A of AB system, ^3J(H,H) = 12.6, 3.4 Hz, 1H), 3.79 (A of AB system, ^3J(H,H) = 12.6, 6.0 Hz, 1H), 3.58 (m, 1H), 3.56 (m, 1H), 1.80 (m, 1H), 1.71 (m, 1H), 1.33 (m, 4H), 0.86 ppm (t, ^3J(H,H) = 7.1 Hz, 3H). ^{13}C NMR (101 MHz, D_2O): δ = 74.1 (C3), 73.4 (C4), 64.4 (C5), 64.2 (C2), 61.0 (C6), 30.0 (C8), 28.4 (C7), 24.5 (C9), 15.7 ppm (C10).

Data for **4o**: The ^{1}H and ^{13}C NMR chemical shifts listed in entry 9.

Data for **4q**: The main ^{1}H and ^{13}C NMR chemical shifts are coincident to those for entry 6 (**4j**).

Entry 11—(2*R*,3*S*,4*R*,5*R*)-2-(hydroxymethyl)pyrrolidine-5-propyl-3,4-diol (4r; 63%), (2*S*,3*S*,4*S*,5*R*)-2-(hydroxymethyl)pyrrolidine-5-propyl-3,4-diol (4s; 28%), *N*-ethyl-(2*R*,3*S*,4*R*,5*R*)-2-(hydroxymethyl)pyrrolidine-5-propyl-3,4-diol (4t; 5%), and *N*-ethyl-(2*S*,3*S*,4*S*,5*R*)-2-(hydroxymethyl)-pyrrolidine-5-propyl-3,4-diol (4u; 5%): Overall yield: 0.181 mmol, 41 mg, 67%; $[\alpha]_D^{20} = +19.6°$ (c = 0.9 in MeOH).

Data for **4r**: ^{1}H NMR (500 MHz, D_2O): δ = 4.28 (t, J = 3.5 Hz, 1H), 4.07 (dd, ^3J(H,H) = 9.2, 3.9 Hz, 1H), 3.95 (A of AB system, ^3J(H,H) = 12.1, 5.1 Hz, 1H), 3.85 (B of AB system, ^3J(H,H) = 12.1, 8.4 Hz, 1H), 3.73 (m, 1H), 3.47 (dt, ^3J(H,H) = 9.3, 5.2 Hz, 1H), 1.77 (m, 2H), 1.36 (m, 4H), 0.86 ppm (t, ^3J(H,H) = 7.2 Hz, 3H). ^{13}C NMR (101 MHz, D_2O): δ = 78.0 (C4), 72.9 (C3), 64.1 (C2), 63.3 (C5), 60.3 (C6), 32.5 (C7), 30.5 (C8), 24.4 (C9), 15.7 ppm (C10).

Data for **4s**: ^{1}H NMR (500 MHz, D_2O): δ = 4.13 (brd, 1H), 4.04 (brs, 1H), 3.91 (A of AB system, ^3J(H,H) = 12.1, 5.1 Hz, 1H), 3.77 (B of AB system, ^3J(H,H) = 12.0, 8.3 Hz, 1H), 3.69 (m, 1H), 3.52 (m, 1H), 1.76 (m, 2H), 1.34 (m, 4H), 0.86 ppm (t, ^3J(H,H) = 7.1 Hz, 3H); ^{13}C NMR (101 MHz, D_2O): δ = 78.8 (C3), 77.9 (C4), 70.2 (C2), 65.6 (C5), 62.4 (C6), 27.4 (C7), 24.5 (C8), 24.5 (C9), 15.7 ppm (C10).

Data for **4t**: The main ^{1}H and ^{13}C NMR chemical shifts are coincident to those for **4g**.

Data for **4u**: The main ^{1}H and ^{13}C NMR chemical shifts are coincident to those for **4f**.

Entry 12—(2*R*,3*S*,4*R*,5*R*)-2-(hydroxymethyl)pyrrolidine-5-butyl-3,4-diol (4r): Yield: 0.087 mmol, 20 mg, 19%; $[\alpha]_D^{20} = +53.2°$ (c = 1.0 in MeOH); the ^{1}H and ^{13}C NMR chemical shifts are coincident to those for entry 11; ESI-TOF: calcd for $[M+H]^+$ $C_9H_{20}NO_3$: 190.1443, found 190.1439.

Entry 13—(2*S*,3*S*,4*S*,5*S*)-2-(hydroxymethyl)pyrrolidine-5-isopropyl-3,4-diol (4v; 84%), *N*-ethyl-(2*S*,3*S*,4*S*,5*S*)-2-(hydroxymethyl)pyrrolidine-5-isopropyl-3,4-diol (4w; 16%): Overall yield: 0.217 mmol, 46 mg, 45%; $[\alpha]_D^{20} = -36.3$ (c = 1.0 in MeOH).

Data for **4v**: ^{1}H NMR (500 MHz, D_2O): δ = 4.03 (m, 2H), 3.88 (A of AB system, ^3J(H,H) = 12.7, 3.8 Hz, 1H), 3.83 (B of AB system, ^3J(H,H) = 12.7, 5.8 Hz, 1H), 3.49 (m, 1H), 3.18 (t, ^3J(H,H) = 8.0 Hz, 1H), 2.05 (m, 1H), 1.04 ppm (dd, ^3J(H,H) = 12.9, 6.8 Hz, 6H); ^{13}C NMR (101 MHz, D_2O): δ = 79.3 (C4), 77.1 (C3), 69.6 (C5), 64.7 (C2), 60.1 (C6), 32.2 (C7), 21.1 (C8), 20.6 ppm (C8′). ESI-TOF: m/z calcd for $[M+H]^+$ $C_9H_{20}NO_3$: 190.1443; found: 190.1437.

Data for **4w**: The main ^{1}H and ^{13}C NMR chemical shifts similar to those for the two conformations of **4ac** (entry 16).

Entry 14—(2*R*,3*S*,4*R*,5*R*)-2-(hydroxymethyl)pyrrolidine-5-isopropyl-3,4-diol (4x): Yield: 0.093 mmol, 21 mg, 50%; $[\alpha]_D^{20} = +38.0$ (c = 0.7 in MeOH); ^{1}H NMR (500 MHz,D_2O): δ = 4.26 (m, 1H), 4.24 (m, 1H), 3.95 (A of AB system, ^3J(H,H) = 12.1, 5.3 Hz, 1H), 3.85 (B of AB system, ^3J(H,H) = 12.1, 8.1 Hz, 1H), 3.70 (m, 1H), 3.27 (t, ^3J(H,H) = 8.5 Hz, 1H), 2.02 (m, 1H), 1.03 ppm (t, ^3J(H,H) = 7.2 Hz, 6H). ^{13}C NMR (101 MHz, D_2O): δ = 76.2 (C4), 73.4 (C3), 68.7 (C5), 64.1 (C2), 60.2 (C6), 32.0 (C7), 21.4 (C8), 20.5 ppm (C8′); ESI-TOF: m/z calcd for $[M+H]^+$ $C_8H_{18}NO_3$: 176.1287; found: 176.1280.

Entry 15—(2*S*,3*S*,4*S*,5*S*)-2-(hydroxymethyl)pyrrolidine-5-((*S*)-*sec*-butyl)-3,4-diol (4y; 55%) and *N*-ethyl-(2*S*,3*S*,4*S*,5*S*)-2-(hydroxymethyl)pyrrolidine-5-((*S*)-*sec*-butyl)-3,4-diol (4z; 45%): Overall yield: 0.151 mmol, 34 mg, 50%; $[\alpha]_D^{20} = -22.9°$ (c = 1.0 in MeOH).

Data for **4y**: ^{1}H NMR (500 MHz, D_2O): δ = 4.08 (t, ^3J(H,H) = 6.8 Hz, 1H), 4.03 (m, 1H), 3.88 (A of AB system, J = 12.7, 3.8 Hz, 1H), 3.83 (B of AB system, ^3J(H,H) = 12.8, 5.7 Hz, 1H), 3.51 (m, 1H), 3.28 (t, ^3J(H,H) = 7.9 Hz, 1H), 1.86 (m, 1H), 1.54 (m, 1H), 1.23 (m, 1H), 1.02 (m, 3H), 0.90 ppm (m, 3H). ^{13}C NMR (101 MHz, D_2O): δ = 79.0 (C4), 77.1 (C3), 68.0 (C5), 64.7 (C2), 60.0 (C6), 38.5 (C7), 28.1 (C8), 16.6 (C10), 12.7 ppm (C9); ESI-TOF: m/z calcd for $[M+H]^+$ $C_9H_{20}NO_3$: 190.1443; found: 190.1434.

Data for **4z**: Two conformations were observed—major conformation I: ^{1}H NMR (500 MHz, D_2O): δ = 4.24 (dd, ^3J(H,H) = 6.8, 4.9 Hz, 1H), 4.15 (t, ^3J(H,H) = 5.5 Hz, 1H), 4.03 (m, 2H), 3.69 (dd, ^3J(H,H) = 11.3, 6.7 Hz, 1H), 3.52 (t, ^3J(H,H) = 5.0 Hz, 1H), 3.45 (m, 1H), 3.36 (m, 1H), 1.99 (m, 1H), 1.52 (m, 1H), 1.38 (t, ^3J(H,H) = 7.1 Hz, 1H), 1.36 (m, 1H), 1.06 (d, ^3J(H,H) = 6.7 Hz, 3H), 0.97 ppm (t, ^3J(H,H) = 7.3 Hz, 3H). ^{13}C NMR (101 MHz, D_2O): δ = 77.6 (C4), 77.6 (C3), 77.3 (C5), 71.0 (C2), 58.9 (C6), 49.6 (C11), 37.6 (C7), 29.3 (C8), 16.1 (C10), 13.8 (C9), 12.7 ppm (C12); minor conformation II: selected signals ^{1}H NMR (500 MHz, D_2O): δ = 4.29 (brs, 1H), 4.09 (brs, 1H), 3.96–3.88 (m, 2H), 3.58 (m, 1H), 3.56 (m, 1H), 3.38–3.27 (m, 1H), 2.08 (m, 1H), 1.38 (m, 3H), 1.37 (m, 1H), 1.33 (m, 1H), 1.10 ppm (m, 6H); ESI-TOF: m/z calcd for $[M+H]^+$ $C_{11}H_{24}NO_3$: 218.1756, found 218.1752.

Entry 16—(2*S*,3*S*,4*S*,5*S*)-2-(hydroxymethyl)pyrrolidine-5-isobutyl-3,4-diol (4aa; 71%), (2*S*,3*S*,4*R*,5*S*)-2-(hydroxymethyl)pyrrolidine-5-isobutyl-3,4-diol (4ab; 6%), and *N*-ethyl-(2*S*,3*S*,4*S*,5*S*)-2-(hydroxymethyl)pyrrolidine-5-isobutyl-3,4-diol (4ac; 23%): Overall yield: 0.129 mmol, 29 mg, 12%; $[\alpha]_D^{20} = -39.3$ (c = 1.0 in MeOH).

Data for **4aa**: ^{1}H NMR (500 MHz, D_2O): δ = 4.03 (t, ^3J(H,H) = 6.9 Hz, 1H), 3.92 (m, 1H), 3.89 (A of AB system, ^3J(H,H) = 12.6, 3.9 Hz, 1H), 3.83 (B of AB system, ^3J(H,H) = 12.7, 6.0 Hz, 1H), 3.53 (m, 1H), 3.48 (m, 1H), 1.74 (m, 1H), 1.67 (m, 1H), 1.63 (m, 1H), 0.92 ppm (m, 6H); ^{13}C NMR (101 MHz, D_2O): δ = 81.8 (C4), 76.9 (C3), 64.8 (C2), 62.4 (C5), 60.6 (C6), 42.0 (C7), 27.1 (C8), 24.7 (C9), 23.6 ppm (C9′). ESI-TOF: m/z calcd for $[M+H]^+$ $C_9H_{20}NO_3$: 190.1443; found: 190.1444.

Data for **4ab**: ^{1}H NMR (500 MHz, D_2O): δ = 4.29 (m, 1H), 4.26 (m, 1H), 3.96 (A of AB system, ^3J(H,H) = 12.6, 3.6 Hz, 1H), 3.83 (B of AB system, ^3J(H,H) = 12.6, 6.0 Hz, 1H), 3.71 (dt, ^3J(H,H) = 7.4 Hz, 1H), 3.58 (ddd, ^3J(H,H) = 9.1, 3.3 Hz, 1H), 1.74 (m, 1H), 1.66 (m, 1H), 1.61 (m, 1H), 0.94 ppm (dd, ^3J(H,H) = 6.3 Hz, 6H); ^{13}C NMR (101 MHz, D_2O): δ = 74.2 (C4), 73.5 (C3), 64.1 (C2), 62.7 (C5), 61.0 (C6), 37.5 (C7), 27.1 (C8), 24.3 (C9′), 24.2 ppm (C9). ESI-TOF: m/z calcd for $[M+H]^+$ $C_9H_{20}NO_3$: 190.1443; found: 190.1439.

Data for **4ac**: Two conformations were observed: major conformation I: ^{1}H NMR (500 MHz, D_2O): δ = 4.25 (brs, 1H), 4.15 (brs, 1H), 4.01 (m, 2H), 3.76 (m, 1H), 3.56 (m, 1H), 3.44 (m, 1H), 3.35 (m, 1H), 1.83 (m, 1H), 1.78 (m, 1H), 1.69 (m, 1H), 1.36 (t, ^3J(H,H) = 4.1 Hz, 1H), 1.02 ppm (t, ^3J(H,H) = 6.5 Hz, 6H); ^{13}C NMR (101 MHz, D_2O): δ = 79.3 (C4), 79.0 (C3), 73.6 (C2), 69.2 (C5), 60.3 (C6), 47.2 (C10), 35.2 (C7), 26.9 (C8), 25.1 (C9′), 23.2 (C9), 12.2 ppm (C11); minor conformation II:

δ = ppm 4.33 (brs, 1H), 4.10 (brs, 1H), 4.08–4.03 (m, 2H), 3.83 (brs, 1H), 3.52 (m, 1H), 3.44 (m, 2H), 1.82 (m, 1H), 1.78 (m, 1H), 1.69 (m, 1H), 1.41 (t, ^3J(H,H) = 6.8 Hz, 1H), 1.02 ppm (t, ^3J(H,H) = 6.5 Hz, 6H); ^{13}C NMR (101 MHz, D_2O): δ = 82.5 (C4), 78.5 (C3), 73.3 (C5), 70.9 (C2), 58.6 (C6), 48.0 (C10), 35.2 (C7), 26.9 (C8), 25.1 (C9′), 23.2 (C9), 12.8 ppm (C11). ESI-TOF: *m*/*z* calcd for $[M+H]^+$ $C_{11}H_{23}NO_3$: 218.1756; found: 217.1752.

Entry 17—(2*R*,3*S*,4*R*,5*R*)-2-(hydroxymethyl)pyrrolidine-5-isobutyl-3,4-diol (4ad; 43%), (2*S*,3*S*,4*S*,5*R*)-2-(hydroxymethyl)pyrrolidine-5-isobutyl-3,4-diol (4ae; 32%), *N*-ethyl-(2*R*,3*S*,4*R*,5*R*)-2-(hydroxymethyl)pyrrolidine-5-isobutyl-3,4-diol (4af; 9%), and *N*-ethyl-(2*S*,3*S*,4*S*,5*R*)-2-(hydroxymethyl)pyrrolidine-5-isobutyl-3,4-diol (4ag; 16%): Reaction at 25 °C; overall yield: 0.067 mmol, 15 mg, 50%.

*Data for **4ad***: ^{1}H NMR (500 MHz, D_2O): δ = 4.27 (t, ^3J(H,H) = 3.5 Hz, 1H), 4.05 (dd, ^3J(H,H) = 9.2, 3.8 Hz, 1H), 3.95 (A of AB system, ^3J(H,H) = 12.1, 5.1 Hz, 1H), 3.85 (B of AB system, ^3J(H,H) = 12.1, 8.3 Hz, 1H), 3.74 (m, 1H), 3.55 (m, 1H), 1.65 (m, 3H), 0.92 ppm (m, 6H); ^{13}C NMR (101 MHz, D_2O): δ = 78.3 (C4), 72.7 (C3), 64.2 (C2), 61.4 (C5), 60.3 (C6), 42.0 (C7), 27.6 (C8), 24.8 (C9), 23.5 ppm (C9′).

*Data for **4ae***: ^{1}H NMR (500 MHz, D_2O): δ = 4.15 (s, 1H), 4.07 (s, 1H), 3.90–3.78 (m, 2H), 3.80 (m, 1H), 3.54 (m, 1H), 1.65 (m, 3H), 0.94 ppm (t, J = 6.4 Hz, 6H); ^{13}C NMR (101 MHz, D_2O): δ = 78.6 (C3), 78.0 (C4), 61.6 (C2), 63.8 (C5), 60.1 (C6), 42.1 (C7), 27.5 (C8), 24.5 (C9), 24.5 ppm (C9′).

*Data for **4af***: The ^{1}H and ^{13}C NMR chemical shifts are coincident to those for **4g**; selected signals: ^{1}H NMR: δ = 4.32 (brs, 1H), 3.46 (m, 1H), 3.26 (m, 1H), 1.28 ppm (t, ^3J(H,H) = 7.5 Hz, 3H).

*Data for **4ag***: The ^{1}H and ^{13}C NMR chemical shifts are coincident to those for **4f**; selected signals: ^{1}H NMR: δ = 4.21 (brs, 1H), 3.40 (m, 1H), 3.20 (m, 1H), 1.30 ppm (t, ^3J(H,H) = 7.6 Hz, 3H).

Entry 18—(2*R*,3*S*,4*R*,5*R*)-2-(hydroxymethyl)pyrrolidine-5-isobutyl-3,4-diol (4ad): Reaction at 4 °C, yield: 0.265 mmol, 60 mg, 16%; $[\alpha]_D^{20} = -57.3$ (c = 0.8 in MeOH); the ^{1}H and ^{13}C NMR chemical shifts are coincident to those for entry 17 (**4ad**); ESI-TOF: *m*/*z* calcd for $[M+H]^+$ $C_9H_{20}NO_3$: 190.1443; found: 190.1444.

Entry 19—(2*S*,3*S*,4*S*,5*S*)-2-(hydroxymethyl)pyrrolidine-5-benzyl-3,4-diol trifluoroacetate salt (4ah): Yield: 0.5 mmol, 170 mg, 10%; $[\alpha]_D^{20} = -45.0°$ (c = 1.0 in MeOH); ^{1}H NMR (500 MHz, CD_3OD): δ = 7.33 (m, 5H), 4.02 (t, ^3J(H,H) = 4.8 Hz, 1H), 3.95 (t, ^3J(H,H) = 5.3 Hz, 1H), 3.86 (A of AB system, ^3J(H,H) = 11.8, 4.1 Hz, 1H), 3.78 (B of AB system, ^3J(H,H) = 11.8, 7.2 Hz, 1H), 3.70 (dt, ^3J(H,H) = 7.7, 5.5 Hz, 1H), 3.57 (m, 1H), 3.26 (A of AB system, ^3J(H,H) = 14.2, 7.6 Hz, 1H), 3.02 ppm (A of AB system, ^3J(H,H) = 14.2, 8.0 Hz, 1H); ^{13}C NMR (101 MHz, CD_3OD): δ = 136.1 (C8), 129.1 (C10), 128.8 (C9), 127.2 (C11), 78.2 (C4), 76.0 (C3), 65.9 (C2), 65.3 (C5), 58.8 (C6), 35.9 ppm (C7); ESI-TOF: *m*/*z* calcd for $[M+H]^+$ $C_{12}H_{18}NO_3$: 224.1287; found: 224.1282.

Entry 20—(2*S*,3*S*,4*R*,5*S*)-2-(hydroxymethyl)pyrrolidine-5-benzyl-3,4-diol (4ai;62%) and (2*R*,3*S*,4*R*,5*S*)-2-(hydroxymethyl)pyrrolidine-5-benzyl-3,4-diol (4aj; 38%): Overall yield: 0.298 mmol, 77 mg, 6%; $[\alpha]_D^{20} = -14.0°$ (c = 1.0 in MeOH).

*Data for **4ai***: ^{1}H NMR (500 MHz, CD_3OD): δ = 7.35 (m, 5H), 4.15 (dd, ^3J(H,H) = 8.6, 3.4 Hz, 1H), 3.94 (brs, 1H), 3.88 (m, 2H), 3.77–3.60 (m, 1H), 3.55 (m, 1H), 3.27 (A of AB system, ^3J(H,H) = 13.6, 8.7 Hz, 1H), 2.96 ppm (B of AB system, ^3J(H,H) = 13.5, 7.3 Hz, 1H); ^{13}C NMR (101 MHz, CD_3OD): δ = 136.4 (C8), 129.1 (C10), 128.7 (C9), 127.1 (C11), 72.1 (C4), 70.5 (C3), 63.2 (C2), 62.3 (C5), 58.5 (C6), 35.4 ppm (C7). ESI-TOF: *m*/*z* calcd for $[M+H]^+$ $C_{12}H_{18}NO_3$: 224.1287; found: 224.1282

*Data for **4aj***: ^{1}H NMR (500 MHz, CD_3OD): δ = 7.26 (m, 5H), 4.41 (dd, ^3J(H,H) = 8.1, 4.5 Hz, 1H), 4.09 (t, ^3J(H,H) = 4.0 Hz, 1H), 3.69 (m, 2H), 3.77 (m, 1H), 3.67 (m, 1H), 3.31 (A of AB system, 1H), 2.98 ppm (B of AB system, ^3J(H,H) = 14.8, 7.1 Hz, 1H); ^{13}C NMR (101 MHz, CD_3OD): δ = 138.0 (C8), 129.0 (C10), 128.7 (C9), 127.1 (C11), 72.1 (C4), 70.3 (C3), 63.0 (C2), 62.2 (C5), 58.7 (C6), 32.1 ppm (C7).

Entry 21—(2*S*,3*S*,4*S*)-2-(hydroxymethyl)pyrrolidine-5-dimetil-3,4-diol (4ak; 83%) and (2*R*,3*S*,4*R*)-2-(hydroxymethyl)pyrrolidine-5-dimetil-3,4-diol (4al; 17%): Overall yield: 0.520 mmol, 103 mg, 21%; $[\alpha]_D^{20} = -38.7°$ (c = 1.3 in MeOH).

*Data for **4ak***: ^{1}H NMR (500 MHz, D_2O): δ = 4.06 (dd, ^3J(H,H) = 7.5, 5.8 Hz, 1H), 3.89 (A of AB system, ^3J(H,H) = 16.4, 3.9 Hz, 1H), 3.89 (s, 1H), 3.81 (B of AB system, ^3J(H,H) = 12.6, 6.7 Hz, 1H), 3.55 (dt, ^3J(H,H) = 7.1, 3.9 Hz, 1H), 1.48 (s, 3H), 1.36 ppm (s, 3H); ^{13}C NMR (101 MHz, D_2O): δ = 83.2 (C4), 77.3 (C3), 67.5 (C5), 64.6 (C2), 61.1 (C6), 26.2 (C7), 22.6 ppm (C7′); ESI-TOF: *m*/*z* calcd for $[M+H]^+$ $C_7H_{16}NO_3$: 162.1130; found: 162.1120.

*Data for **4al***: ^{1}H NMR (500 MHz, D_2O): δ = 4.04 (dd, ^3J(H,H) = 5.5, 1.9 Hz, 1H), 3.95 (m, 1H), 3.94–3.85 (m, 2H), 3.47 (brq, ^3J(H,H) = 9.8, 5.3 Hz, 1H), 1.41 (s, 3H), 1.38 ppm (s, 3H); ^{13}C NMR (101 MHz, D_2O): δ = 83.2 (C4), 78.5 (C3), 75.5 (C2), 67.5 (C5), 60.6 (C6), 21.0 (C7), 20.7 ppm (C7′).

Entry 22—(2*R*,3*S*,4*R*)-2-(hydroxymethyl)pyrrolidine-5-dimetil-3,4-diol (4am) and (2*S*,3*S*,4*R*)-2-(hydroxymethyl)pyrrolidine-5-dimetil-3,4-diol (4al): Yield: 0.136 mmol, 27 mg, 12%; $[\alpha]_D^{20} = +5°$ (c = 1 in MeOH).

*Data for **4am***: ^{1}H NMR (500 MHz, D_2O): δ = 4.39 (t, ^3J(H,H) = 4.7 Hz, 1H), 4.33 (dd, ^3J(H,H) = 4.5, 8.4 Hz, 1H), 3.93 (d, ^3J(H,H) = 4.5 Hz, 1H), 3.82 (A of AB system, 1H), 3.73 (B of AB system, 1H), 3.70 (m, 1H), 1.32 (s, 3H), 1.29 ppm (s, 3H); ^{13}C NMR (101 MHz, D_2O): δ = 79.31 (C4), 72.9 (C3), 67.5 (C5), 62.2 (C2), 60.3 (C6), 26.8 (C7), 23.6 ppm (C7′); ESI-TOF: *m*/*z* calcd for $[M+H]^+$ $C_7H_{16}NO_3$: 162.1130; found: 162.1124.

*Data for **4al***: The chemical shifts differ slightly from those of entry 21: ^{1}H NMR (500 MHz, D_2O): δ = 4.33 (dd, J = 4.5, 8.9 Hz, 1H), 3.84 (m, 1H), 3.78–3.70 (m, 2H), 3.50 (m, 1H), 1.33 (s, 3H), 1.28 ppm (s, 3H); ^{13}C NMR (101 MHz, D_2O): δ = 78.7 (C4), 72.9 (C3), 69.2 (C5), 65.2 (C2), 60.7 (C6), 26.1 (C7), 22.8 ppm (C7′).

Purification by ion exchange chromatography: The mixtures of entries 3, 6, 15, and 16 (10–20 mg, Table 2) were separated by ion exchange chromatography on a FPLC system following a method described by Asano et al.[71] CM-Sepharose CL-6B (Amersham Pharmacia) in NH_4^+ form stationary phase was packed into a glass column (160 × 20 mm) to give a final bed volume of 50 mL. The flow rate was 0.9 mL min^{-1}. The CM-Shepharose-NH_4^+ was washed initially with H_2O. Then, an aqueous solution of the crude material at pH 7 was loaded onto the column. Minor colored impurities were washed away with H_2O (150 mL, 3 bed volumes). The retained compounds were eluted with aqueous NH_4OH (0.01 M): entry 2 (20 mg) compounds: **4b** (elution volume 116 mL, 5 mg); **4c** (elution volume 156 mL, 2 mg); entry 3 (15 mg) compounds: **4d** (elution volume 136 mL, 4 mg), **4e** (elution volume 162 mL, 2 mg), **4f** (elution volume 104 mL, 2 mg), **4g** (elution volume 143 mL, 1 mg); entry 6 (20 mg) compounds: **4i** (elution volume 204 mL, 4 mg); **4j** (elution volume 224 mL, 1 mg); entry 15 (15 mg) compounds: **4y** (elution volume 91 mL, 9 mg), **4z** (elution volume 104 mL, 3 mg); entry 16 (18 mg) compounds: **4aa** (elution volume 84 mL, 7 mg), **4ab** (elution volume 195 mL, 3 mg), **4ac** (elution volume 97 mL, 2 mg). In each case, the operation was repeated until the whole crude was consumed. Pure fractions were pooled and lyophilized. Physical and NMR data are listed above. ^{1}H and ^{13}C NMR spectra are given in Supporting Information.

Enzymatic inhibition assays: Commercial glycosidase solutions were prepared with the appropriate buffer and incubated in 96-well plates at 37 °C without (control) or with inhibitor (1.6–4.2 nM) for 3 min for α-D-glucosidase, β-D-glucosidase, α-D-mannosidase, α-L-rhamnosidase, and α-L-fucosidase, and 5 min for β-D-galactosidase. After addition of the corresponding substrate solution, incubations were prolonged for different time periods: 10 min for α-D-glucosidase, 3 min for β-D-glucosidase, 6 min for α-D-mannosidase, 5 min for α-L-rhamnosidase, 7 min for α-L-fucosidase, and 16 min for β-D-galactosidase and stopped by addition of Tris solution (50 μL, 1 M) or glycine buffer (180 μL, 100 mM, pH 10), depending on the enzymatic inhibition assay. The amount of *p*-nitrophenol formed was determined at 405 nm with UV/VIS Spectramax Plus (Molecular Devices Corporation) spectrophotometer. For α-D-glucosidase from rice, the activity was determined with *p*-nitrophenyl-α-D-glucopyranoside (1 mM) in sodium acetate buffer (50 mM, pH 5.0). β-D-Glucosidase activity was determined with *p*-nitrophenyl-β-D-glucopyranoside (1 mM) in sodium acetate buffer (100 mM, pH 5.0). β-D-Galactosidase activity was determined with *p*-nitrophenyl-β-D-galactopyranoside (1 mM) in sodium phosphate buffer (100 mM, 0.1 mM $MgCl_2$, pH 7.2). α-D-Mannosidase ac-

tivity was determined with *p*-nitrophenyl-α-D-mannopyranoside (1 mM) in sodium acetate buffer (50 mM, pH 5.0). α-L-Rhamnosidase activity was determined with *p*-nitrophenyl-α-D-rhamnopyranoside (1 mM) in sodium acetate buffer (50 mM, pH 5.0). α-L-Fucosidase activity was determined with *p*-nitrophenyl-α-D-fucopyranoside (0.15 mM) in sodium acetate buffer (50 mM, pH 5.0). The commercial glycosidase solutions were prepared as follows: α-D-glucosidase $(NH_4)_2SO_4$ suspension (100 μL) in buffer (5 mL); β-D-glucosidase: (0.1 mg mL^{-1} buffer), β-D-galactosidase from *Aspergillus oryzae* (0.5 mg mL^{-1} buffer), α-L-rhamnosidase (naringinase) (0.3 mg mL^{-1} buffer); α-D-mannosidase $(NH_4)_2SO_4$ suspension (25 μL) in buffer (10 mL); β-D-galactosidase from bovine liver (0.1 mg mL^{-1} buffer), and α-L-fucosidase $(NH_4)_2SO_4$ suspension (33 μL) in buffer (10 mL).

Kinetics of inhibition: The nature of the inhibition against enzymes and the K_i values were determined from the Lineweaver–Burk or Dixon plots.

Computational methods: All molecular simulations were conducted with the program MOE (v. 2007.09 and 2008.10, Chemical Computing Group, Montreal). The implemented MMFF94x force field, a modified version of the MMFF94s force field,[72,73] was used in all protein–ligand and ligand alone calculations. The electrostatic interactions were approximated using the generalized Born/Volume Integral (GB/VI) methodology,[74] without cutoffs when no protein was implied or with a smoothed cutoff between 14–15 Å when there was a protein in the system. The coordinates of the complex *E. coli* rhamnulose-1-phosphate aldolase with phosphoglycolohydroxamic acid (PGH), *Thermotoga maritima* α-L-fucosidase-fucosyl fluoride complex, α-L-rhamnosidase from *Bacillus* sp. GL1 and α-D-mannosidase from *Drosophila melanogaster* were obtained from the Protein Data Bank[75] at Brookhaven National Laboratory (entries 1GT7, 1L9, 2OKX, and 1HXK respectively). The protocols used to determine the lowest energy conformations for the aldol adducts in free state and as complexes with the RhuA active center were the same as those previously reported.[24,40] For the free adducts, starting from an initially optimized structure, a systematic conformational search was run in which every non-terminal single bond was rotated in 60–120° steps. The conformations generated for each compound were then minimized and ranked according to their energy. To confirm the nature of the lowest energy conformer determined, a subsequent stochastic conformational search was run in which the conformational space of the molecules was explored by random rotation of bonds and simultaneous Cartesian perturbation. The conformations thus generated were minimized and checked to determine if they were duplicates, within a RMS tolerance (0.1 Å), of previously generated conformations. The process was finished when the number of failures to find new conformations exceeded a large enough number (1000) of attempts. The adducts bound in the active center of RhuA were first built by modifying the structure of the PGH molecule included in PDB 1GT7. After a preliminary minimization, the conformational space of the ligands was explored by running a stochastic conformational search, as described above, to find the lowest energy minima. During this conformational search, a restraint was imposed to keep the coordination of the DHAP moiety to the Zn^{2+}. All the conformations obtained were further minimized without restraints and keeping the protein rigid.

The docking calculations to determine the binding modes of the pyrrolidine inhibitors to the active site of α-L-fucosidase, α-L-rhamnosidase, and α-D-mannosidase were performed with the docking application included in MOE. Previous to these docking simulations, the structures of the proteins were prepared by removing all the solvent molecules and ligands, adding hydrogen atoms, and minimizing the energy using the Amber99 force field[76,77] with implicit water solvation conditions (GB/VI), to remove any steric clashes. Furthermore, the structure of *T. maritima* α-L-fucosidase was modified in the following way. From the two chains contained in the PDB structure, chain A, which contains a molecule of fucosyl fluoride in the active center of the enzyme, was used as starting point to build the complete sequence of the protein. For that purpose, the coordinates of the inhibitor at the active site were removed, the lacking residues 1–6, 47–55, 267–274, 297–300, and 449 were introduced in the protein sequence, and their structure was modeled and refined using the Homology Modeling module contained in MOE. The Amber99 force field and the default parameters implemented in the program were used for the energetic calculations. Thus, ten models were generated that were minimized and scored. The Ramachandran plots were used to asses the quality of the models. The best scored model was used to carry out the subsequent docking experiments. The protonation state of every residue in the proteins was generally determined with the Protonate 3D application implemented in MOE.[78] Protonate 3D solves the macromolecular protonation state assignment problem by selecting a protonation state for each chemical group that minimizes the total free energy of the system. In the particular case of the α-L-fucosidase, which contains three residues of histidine in the active center (H34, H128 and H129), the eight possible protonation states derived from considering each His residue as neutral or charged were manually generated and the docking experiments were performed with the eight structures for the protein. All docking experiments were carried out allowing full flexibility for the ligands and treating the proteins as rigid. To ensure an appropriate search of the conformational space of the pyrrolidine ring, a conformational search centered on the ring was carried out previous to the docking. In this way, several ring conformers were generated for each compound and all of them were used in independent docking runs. The docking protocol implied several stages:

1. *Conformer generation*: Only the dihedral angles of non-ring bonds were varied and up to 5000 conformations/ligand were generated.
2. *Placement*: Up to 1000 poses were generated for each ligand using the alpha PMI method, in which ligands are placed by aligning randomly their principal moments of inertia in the receptor site.
3. *Scoring*: The London dG scoring function implemented in MOE was used as a crude estimation of the free energy of binding of the ligand from a given pose. In this step up to 50 poses, after removal of duplicates, were obtained for each ligand.
4. *Refinement*: Energy minimization of the system was carried out using the MMFF94x forcefield and keeping the protein rigid.
5. *Re-scoring*: Poses were re-scored by determining the MM/GBVI non-bonded interaction energy, which comprises van der Waals, Coulomb and generalized Born implicit solvent interaction energies, between the receptor and the ligand.

Interaction diagrams were built with MOE for the best docked poses obtained for some of the inhibitors (see Supporting Information).

Acknowledgements

This work was supported by the Spanish MEC CTQ2006-01345/BQU, La Marató de TV3 foundation (Ref.: 050931), Generalitat de Catalunya (DURSI 2005-SGR-00698 and Grant 2005SGR05-01063), and ESF projects COST D25/0006/05 and CM0701. J. Calveras acknowledges the CSIC for the I3P predoctoral scholarship.

[1] N. Asano, R. J. Nash, R. J. Molyneux, G. W. J. Fleet, *Tetrahedron: Asymmetry* **2000**, *11*, 1645–1680.
[2] P. Compain, O. R. Martin, *Bioorg. Med. Chem.* **2001**, *9*, 3077–3092.
[3] C. R. Bertozzi, L. L. Kiessling, *Science* **2001**, *291*, 2357–2364.
[4] A. Varki, *Cell* **2006**, *126*, 841–845.
[5] K. M. Koeller, C. H. Wong, *Nat. Biotechnol.* **2000**, *18*, 835–841.
[6] R. K. Yu, M. Yanagisawa, *J. Neurochem.* **2007**, *103*, 39–46.
[7] N. Asano, *J. Enzyme Inhib.* **2000**, *15*, 215–234.
[8] A. A. Watson, G. W. J. Fleet, N. Asano, R. J. Molyneux, R. J. Nash, *Phytochemistry* **2001**, *56*, 265–295.
[9] T. D. Butters, R. A. Dwek, F. M. Platt, *Curr. Top. Med. Chem.* **2003**, *3*, 561–574.
[10] P. Compain, O. R. Martin, *From Synthesis Iminosugars to Therapeutic Applications*, Wiley, New York, **2007**, p. 467.

[11] T. M. Wrodnigg, A. J. Steiner, B. J. Ueberbacher, *Anti-Cancer Agents Med. Chem.* **2008**, *8*, 77–85.
[12] T. D. Heightman, A. T. Vasella, *Angew. Chem.* **1999**, *111*, 794–815; *Angew. Chem. Int. Ed.* **1999**, *38*, 750–770.
[13] A. Vasella, G. J. Davies, M. Bohm, *Curr. Opin. Chem. Biol.* **2002**, *6*, 619–629.
[14] L. Cipolla, B. La Ferla, F. Nicotra, *Curr. Top. Med. Chem.* **2003**, *3*, 485–511.
[15] T. Ayad, Y. Genisson, M. Baltas, *Curr. Org. Chem.* **2004**, *8*, 1211–1233.
[16] M. Sugiyama, W. Greenberg, C. H. Wong, *J. Synth. Org. Chem. Jpn.* **2008**, *66*, 605–615.
[17] J.-B. Behr, R. Plantier-Royon, *Recent Res. Dev. Org. Chem.* **2006**, *10*, 23–52.
[18] L. Cipolla, B. La Ferla, M. Gregori, *Comb. Chem. High Throughput Screening* **2006**, *9*, 571–582.
[19] P. Greimel, J. Spreitz, F. K. Sprenger, A. E. Stutz, T. M. Wrodnigg, *Org. Chem. Sugars* **2006**, 383–424.
[20] A. Kato, N. Kato, E. Kano, I. Adachi, K. Ikeda, L. Yu, T. Okamoto, Y. Banba, H. Ouchi, H. Takahata, N. Asano, *J. Med. Chem.* **2005**, *48*, 2036–2044.
[21] H. Ouchi, Y. Mihara, H. Watanabe, H. Takahata, *Tetrahedron Lett.* **2004**, *45*, 7053–7056.
[22] N. Asano, K. Ikeda, L. Yu, A. Kato, K. Takebayashi, I. Adachi, I. Kato, H. Ouchi, H. Takahata, G. W. J. Fleet, *Tetrahedron: Asymmetry* **2005**, *16*, 223–229.
[23] H. Takahata, Y. Banba, H. Ouchi, H. Nemoto, A. Kato, I. Adachi, *J. Org. Chem.* **2003**, *68*, 3603–3607.
[24] L. Espelt, J. Bujons, T. Parella, J. Calveras, J. Joglar, A. Delgado, P. Clapés, *Chem. Eur. J.* **2005**, *11*, 1392–1401.
[25] L. Espelt, T. Parella, J. Bujons, C. Solans, J. Joglar, A. Delgado, P. Clapés, *Chem. Eur. J.* **2003**, *9*, 4887–4899.
[26] C. Saotome, C. H. Wong, O. Kanie, *Chem. Biol.* **2001**, *8*, 1061–1070.
[27] C. Y. Wu, C. F. Chang, J. S. Y. Chen, C. H. Wong, C. H. Lin, *Angew. Chem.* **2003**, *115*, 4809–4812; *Angew. Chem. Int. Ed.* **2003**, *42*, 4661–4664.
[28] I. Robina, A. J. Moreno-Vargas, J. G. Fernandez-Bolanos, J. Fuentes, R. Demange, P. Vogel, *Bioorg. Med. Chem. Lett.* **2001**, *11*, 2555–2559.
[29] A. T. Carmona, J. Fuentes, I. Robina, E. R. Garcia, R. Demange, P. Vogel, A. L. Winters, *J. Org. Chem.* **2003**, *68*, 3874–3883.
[30] A. T. Carmona, F. Popowycz, S. Gerber-Lemaire, E. Rodriguez-Garcia, C. Schutz, P. Vogel, I. Robina, *Bioorg. Med. Chem.* **2003**, *11*, 4897–4911.
[31] F. Popowycz, S. Gerber-Lemaire, C. Schutz, P. Vogel, *Helv. Chim. Acta* **2004**, *87*, 800–810.
[32] T. D. Butters, L. A. G. M. Van den Broek, G. W. J. Fleet, T. M. Krulle, M. R. Wormald, R. A. Dwek, F. M. Platt, *Tetrahedron: Asymmetry* **2000**, *11*, 113–124.
[33] A. J. Moreno-Vargas, I. Robina, R. Demange, P. Vogel, *Helv. Chim. Acta* **2003**, *86*, 1894–1913.
[34] T. M. Wrodnigg, S. G. Withers, A. E. Stutz, *Bioorg. Med. Chem. Lett.* **2001**, *11*, 1063–1064.
[35] C. Mattos, D. Ringe, *Curr. Opin. Struct. Biol.* **2001**, *11*, 761–764.
[36] C. Mattos, C. R. Bellamacina, E. Peisach, A. Pereira, D. Vitkup, G. A. Petsko, D. Ringe, *J. Mol. Biol.* **2006**, *357*, 1471–1482.
[37] L. Espelt, P. Clapés, J. Esquena, A. Manich, C. Solans, *Langmuir* **2003**, *19*, 1337–1346.
[38] T. Suau, G. Alvaro, M. D. Benaiges, J. Lopez-Santín, *Biotechnol. Bioeng.* **2006**, *93*, 48–55.
[39] M. L. Gutiérrez, X. Garrabou, E. Agosta, S. Servi, T. Parella, J. Joglar, P. Clapés, *Chem. Eur. J.* **2008**, *14*, 4647–4656.
[40] J. Calveras, J. Bujons, T. Parella, R. Crehuet, L. Espelt, J. Joglar, P. Clapés, *Tetrahedron* **2006**, *62*, 2648–2656.
[41] A. Jiménez, P. Clapés, R. Crehuet, *Chem. Eur. J.* **2009**, *15*, 1422–1428.
[42] M. Hayashi, H. Kawabata, *Adv. Chem. Res.* **2006**, *1*, 45–62.
[43] A full study on the inhibition activity against α-L-fucosidase from bovine kidney of **5** and **6** and its diasteromerically related pyrrolidine isomers will be published elsewhere.
[44] In our hands, the inhibitory activity of **5** was higher than the value previously reported by Wang et al.[48]
[45] M. Joubert, A. Defoin, C. Tarnus, J. Streith, *Synlett* **2000**, 1366–1368.
[46] N. Asano, K. Yasuda, H. Kizu, A. Kato, J.-Q. Fan, R. J. Nash, G. W. J. Fleet, R. J. Molyneux, *Eur. J. Biochem.* **2001**, *268*, 35–41.
[47] M. Dubernet, A. Defoin, C. Tarnus, *Bioorg. Med. Chem. Lett.* **2006**, *16*, 1172–1174.
[48] Y. F. Wang, D. P. Dumas, C. H. Wong, *Tetrahedron Lett.* **1993**, *34*, 403–406.
[49] In a control experiment the known α-L-fucosidase inhibitor, 1-deoxy-l-fuconojirimycin, was assayed giving a value of $K_i = 4.9$ nM in good agreement with that reported in the literature.[45]
[50] E. Moreno-Clavijo, A. T. Carmona, Y. Vera-Ayoso, A. J. Moreno-Vargas, C. Bello, P. Vogel, I. Robina, *Org. Biomol. Chem.* **2009**, *7*, 1192–1202.
[51] A. J. Moreno-Vargas, A. T. Carmona, F. Mora, P. Vogel, I. Robina, *Chem. Commun.* **2005**, 4949–4951.
[52] C. Chevrier, D. LeNouen, M. Neuburger, A. Defoin, C. Tarnus, *Tetrahedron Lett.* **2004**, *45*, 5363–5366.
[53] C. Laroche, J. B. Behr, J. Szymoniak, P. Bertus, C. Schutz, P. Vogel, R. Plantier-Royon, *Bioorg. Med. Chem.* **2006**, *14*, 4047–4054.
[54] G. Sulzenbacher, C. Bignon, T. Nishimura, C. A. Tarling, S. G. Withers, B. Henrissat, Y. Bourne, *J. Biol. Chem.* **2003**, *279*, 13119–13128.
[55] T. M. Gloster, P. Meloncelli, R. V. Stick, D. Zechel, A. Vasella, G. J. Davies, *J. Am. Chem. Soc.* **2007**, *129*, 2345–2354.
[56] T. M. Chapman, S. Courtney, P. Hay, B. G. Davis, *Chem. Eur. J.* **2003**, *9*, 3397–3414.
[57] J. H. Kim, M. J. Curtis-Long, W. D. Seo, J. H. Lee, B. W. Lee, Y. J. Yoon, K. Y. Kang, K. H. Park, *Bioorg. Med. Chem. Lett.* **2005**, *15*, 4282–4285.
[58] L. Provencher, D. H. Steensma, C.-H. Wong, *Bioorg. Med. Chem.* **1994**, *2*, 1179–1188.
[59] Z. Cui, Y. Maruyama, B. Mikami, W. Hashimoto, K. Murata, *J. Mol. Biol.* **2007**, *374*, 384–398.
[60] W. Hashimoto, H. Nankai, B. Mikami, K. Murata, *J. Biol. Chem.* **2003**, *278*, 7663–7673.
[61] S. P. Kawatkar, D. A. Kuntz, R. J. Woods, D. R. Rose, G. J. Boons, *J. Am. Chem. Soc.* **2006**, *128*, 8310–8319.
[62] D. A. Kuntz, W. Z. J. Guo, D. R. Rose, G.-J. Boons, *ChemBioChem* **2009**, *10*, 268–277.
[63] D. A. Kuntz, C. A. Tarling, S. G. Withers, D. R. Rose, *Biochemistry* **2008**, *47*, 10058–10068.
[64] W. Zhong, D. A. Kuntz, B. Ember, H. Singh, K. W. Moremen, D. R. Rose, G. J. Boons, *J. Am. Chem. Soc.* **2008**, *130*, 8975–8983.
[65] B. L. Cantarel, P. M. Coutinho, C. Rancurel, T. Bernard, V. Lombard, B. Henrissat, *Nucleic Acids Res.* **2009**, *37*, D233–D238.
[66] S. Howard, S. He, S. G. Withers, *J. Biol. Chem.* **1998**, *273*, 2067–2072.
[67] Although the bound conformation of mannostatin A in structure 2F7O shows the thiomethyl group oriented away from the hydrophobic pocket constituted by residues F206, W415, and Y727 and towards the hydrophilic environment, a recent paper[62] from the group that originally deposited the structure points out that this was actually due to an experimental artifact and that a later structural determination under different conditions showed that the actual orientation of the thiomethyl group is towards the above mentioned hydrophobic pocket.
[68] S.-H. Jung, J.-H. Jeong, P. Miller, C.-H. Wong, *J. Org. Chem.* **1994**, *59*, 7182–7184.
[69] M. Ocejo, J. L. Vicario, D. Badia, L. Carrillo, E. Reyes, *Synlett* **2005**, 2110–2112.
[70] F. Effenberger, A. Straub, *Tetrahedron Lett.* **1987**, *28*, 1641–1644.
[71] N. Asano, H. Kuroi, K. Ikeda, H. Kizu, Y. Kameda, A. Kato, I. Adachi, A. A. Watson, R. J. Nash, G. W. J. Fleet, *Tetrahedron: Asymmetry* **2000**, *11*, 1–8.

[72] T. A. Halgren, *J. Comput. Chem.* **1999**, *20*, 730–748.
[73] T. A. Halgren, *J. Comput. Chem.* **1999**, *20*, 720–729.
[74] P. Labute, *J. Comput. Chem.* **2008**, *29*, 1693–1698.
[75] H. M. Berman, J. Westbrook, Z. Feng, G. Gilliland, T. N. Bhat, H. Weissig, I. N. Shindyalov, P. E. Bourne, *Nucleic Acids Res.* **2000**, *28*, 235–242.
[76] W. D. Cornell, P. Cieplak, C. I. Bayly, I. R. Gould, K. M. Merz, D. M. Ferguson, D. C. Spellmeyer, T. Fox, J. W. Caldwell, P. A. Kollman, *J. Am. Chem. Soc.* **1995**, *117*, 5179–5197.
[77] J. Wang, P. Cieplak, P. A. Kollman, *J. Comput. Chem.* **2000**, *21*, 1049–1074.
[78] P. Labute, *Proteins* **2009**, *75*, 187–205.

Received: March 31, 2009
Published online: July 3, 2009

